On the Modelling of Gyroplane Flight Dynamics

Dr Stewart Houston

Dr Douglas Thomson

Aerospace Sciences Research Division

School of Engineering

University of Glasgow

Glasgow

G12 8QQ

On the Modelling of Gyroplane Flight Dynamics

Abstract

The study of the gyroplane, with a few exceptions, is largely neglected in the literature which is indicative of a niche configuration limited to the sport and recreational market where resources are limited. However the contemporary needs of an informed population of owners and constructors, as well as the possibility of a wider application of such low-cost rotorcraft in other roles, suggests that an examination of the mathematical modelling requirements for the study of gyroplane flight mechanics is timely. Rotorcraft mathematical modelling has become stratified in three levels, each one defining the inclusion of various layers of complexity added to embrace specific modelling features as well as an attempt to improve fidelity. This paper examines the modelling of gyroplane flight mechanics in the context of this complexity, and shows that relatively simple formulations are adequate for capturing most aspects of gyroplane trim, stability and control characteristics. In particular the conventional 6 degree-of-freedom model structure is suitable for the synthesis of models from flight test data as well as being the framework for reducing the order of the higher levels of modelling. However, a high level of modelling can be required to mimic some aspects of behaviour observed in data gathered from flight experiments and even then can fail to capture other details. These limitations are addressed in the paper. It is concluded that the mathematical modelling of gyroplanes for the simulation and analysis of trim, stability and control presents no special difficulty and the conventional techniques, methods and formulations familiar to the rotary-wing community are directly applicable.

Keywords: rotary-wing; gyroplane; flight dynamics; simulation

Nomenclature

A	linearised model system matrix; rotor disc area, *m²*
A_{11}, *etc*	minors of A
a_0	blade element lift coefficient at zero angle of attack
a_0	blade element lift curve slope, *1/rad*
a_x^{hinge}, a_z^{hinge}	hinge acceleration components, *m/s²*
B	linearised model control matrix
B_1, B_2	minors of B
b	number of blades
dD	blade element drag, *N*
dL	blade element lift, *N*
dQ	blade element torque, *N*
$I_{flap}, I_{pitch}, I_{lag}$	blade moments of inertia, *kgm²*
i	imaginary operator
$\boldsymbol{L}$	dynamic inflow model static gain matrix; rotor moment vector, *Nm*
L_u, etc	derivative - rolling moment with respect to u, *1/ms, etc*
L_{aero}	aerodynamic rolling moment, *Nm*
M_{aero}	aerodynamic pitching moment, *Nm*
M_u, etc	derivative - pitching moment with respect to u, *1/ms, etc*
$M_{flap}^{bl}, M_{pitch}^{bl}, M_{lag}^{bl}$	blade flap, feather and and lag moments, *Nm*
m_{bl}	blade mass, *kg*
$\dot{m}$	inflow, *m/s*
N_u, etc	derivative - yawing moment with respect to u, *1/ms, etc*
p, q, r	body axes angular velocity components, *rad/s*
R	rotor radius, *m*
$Re[\,], Im[\,]$	real and imaginary components of [ ]
r	radial position on disc or blade, *m*

$\boldsymbol{r}_{cg}$	position of centre of mass, body axes, *m*
$\boldsymbol{r}_{hinge}$	position of flap, lag and feather hinge, rotor axes, *m*
$\boldsymbol{r}_{hub}$	position of rotor hub, body axes, *m*
S	vorticity source, *1/s²*
s	rotor solidity
T	rotor thrust, *N*
T_{prop}	propeller thrust, *N*
T_{aero}	aerodynamic thrust moment, *N*
T_1, T_2, T_3	transformation matrices
u, v, w	translational velocity components, body axes, *m/s*
$u(\omega)$	Fourier-transformed control vector
$u_{probe}, v_{probe}, w_{probe}$	translational velocity components at air data probe, body axes, *m/s*
$\boldsymbol{u}$	control vector
$u_{hub}, v_{hub}, w_{hub}$	rotor hub velocities in non-rotating reference frame, *m/s*
V_f	airspeed, *m/s*
$v_i(r, \psi)$	induced velocity at position (r, ψ), *m/s*
v_{i_m}	momentum induced velocity, *m/s*
$v_{i_0}, v_{1_s}, v_{1_c}$	components of induced velocity, *m/s*
v_m	wake mass flow velocity, *m/s*
v_T	wake velocity, *m/s*
$\boldsymbol{X}$	rotor force vector, *N*
$\boldsymbol{X}_{elem}, \boldsymbol{X}_{elem}^{aero}, \boldsymbol{X}_{elem}^{inertial}$	blade element contributions to rotor force - total, aerodynamic, inertial, *N*
X_u, etc	derivative – longitudinal force with respect to u, *1/s, etc*
$\boldsymbol{x}$	state vector
$x(\omega)$	Fourier-transformed state vector
x_{blade}	blade Ox axis
x_R	horizontal distance of rotor hub ahead of c.g., *m*

$x_{vane}, y_{vane}, z_{vane}$	air data probe location, body axes, *m*
$\boldsymbol{x}_1, \boldsymbol{x}_2$	subspace of linearised model state vector
Y_u, etc	derivative – lateral force with respect to u, *1/s, etc*
y_{cg}^{bl}	distance of blade centre of mass from hinge, *m*
Z_u, etc	derivative – normal force with respect to u, *1/s, etc*
z_{prop}	vertical distance of propeller thrust line above c.g., *m*
z_R	vertical distance of rotor hub above c.g., *m*
α_D	rotor disc angle of attack, *rad*
$\alpha_{vane}, \beta_{vane}$	angles of attack and sideslip at air data probe, *rad*
β	blade flapping angle, *rad*
$\beta_0, \beta_{1_s}, \beta_{1_c}$	disc coning, lateral and longitudinal tilt, *rad*
Δf	frequency increment, *rad/s*
Δt	time increment, *s*
δ	blade element drag coefficient
θ	pitch attitude; blade feather angle, *rad*
$\eta_c, \eta_s, \eta_{rudder}, \eta_{prop}$	control angles - lateral and longitudinal rotor tilt, rudder and propeller, *rad*
$\lambda_{cone}, \lambda_{adv}, \lambda_{reg}$	stability roots of the coning, advancing and regressing flap modes
v	flow velocity, *m/s*
ρ	air density, *kg/m^3*
ϕ	roll attitude; inflow angle, *rad*
$[\mathbf{T}]$	time constant matrix, *sec*
χ	wake skew angle, *rad*
ψ	azimuthal position on rotor hub (zero to rear); yaw angle, *rad*
Ω	rotorspeed, *rad/s*
ω	frequency, *rad/s;* flow vorticity, *1/s*
$\omega_x^{bl}, \omega_y^{bl}, \omega_z^{bl}$	blade angular velocities, *rad/s*

Introduction

There is little application of rotorcraft mathematical modelling techniques to the study of gyroplane flight mechanics; indeed there is little on the study of autorotation other than examination of fundamental concepts found in rotorcraft textbooks and some references of historical significance. Prior to 1992 when the UK Civil Aviation Authority (CAA) started its programme of research into gyroplane airworthiness and flight safety, only two recorded applications of contemporary rotorcraft flight mechanics modelling techniques to the gyroplane problem are to be found [1, 2]. The first was conducted in response to a fatal accident in an attempt to understand the behaviour of the aircraft; the second was a postgraduate dissertation. Both used a disc, rather than individual blade, representations of the rotor and could therefore be classified as Level 1 models. This has benefits in terms of simplicity of formulation, understanding and interpretation but limitations in terms of the level of approximation necessary to achieve solutions.

The CAA study required an examination of a number of issues associated with flight mechanics modelling of gyroplanes, [3 - 12] encompassing both theoretical modelling as well as derivation from flight test data. An analytical model was not specifically prepared for gyroplane analyses; rather, a generic rotorcraft simulation code was populated with configuration-specific data. In principle the only salient difference in gyroplane modelling is the inclusion of the rotorspeed variable as a degree of freedom, [4]. Latterly a flowfield code was incorporated, albeit still with rigid hinged blades, [13]. This allowed the study of aerodynamic interactions between the rotor, propeller and empennage, [12]. Analysis of steady flight test data included synthesis of inflow models from blade flapping measurements [14], providing some degree of validation of the commonly-used dynamic inflow model, [15], in the context of autorotation. The outcome of this work, conducted over a period of 16 years, was support of the CAA's management of gyroplane airworthiness and flight safety [16].

This activity appeared to stimulate broader interest in gyroplane flight, either to support potential applications of the configuration, as reviews of historical data in a contemporary context or simply

for technical curiosity, [17-37]. There is much of general technical interest, in particular review items by McCormick [24], Leishman [36] and the splendid volume by Harris [37]. However studies specifically addressing flight dynamics modelling are rare, [29, 38, 39]. The former is primarily concerned with the behaviour of the rigid-body modes of motion, while the latter two address validation against flight test data, particularly in terms of trim and time response to control inputs.

The objective of this Paper is to assess the mathematical modelling requirements for simulation of gyroplane flight mechanics for stability and control analyses. In particular, the appropriateness or otherwise of simplified models is addressed, especially with reference to those higher order dynamics found to be of significance in rotorcraft modelling such as those associated with inflow and flapping. The usefulness of the conventional 6 degree-of-freedom, linearised small-perturbation theory structure is a primary focus given its timeless and all-pervading role in understanding the behaviour of flight vehicles.

The paper begins with a review of established methods of modelling rotary-wing aircraft. The focus of this initially is on the methods used in helicopter simulation as naturally, the vast majority of relevant research has been associated with this class of vehicle. The discussion is then broadened to include the gyroplane (or autogyro) a qualitative discussion being followed by a detailed description of the method used to develop the models used in this paper. A comprehensive nonlinear model is developed and this is the primary source for other linear reduced order models used in the analysis in this paper. Available flight data from two gyroplane types is used to validate these models firstly by comparison of trim and response to controls from flight and model, and subsequently using system identification to extract linear models from the test data. The stability derivatives extracted from flight data are compared with those calculated from numerical differentiation of the nonlinear

model. In the Analysis section a further simplified model is introduced and validated. This model proves useful in analysing the results from the more complex nonlinear model. The main focus of the analysis is the identification of deficiencies with current models and the improvements needed to better capture the flight dynamics of rotary-wing vehicles in autorotative flight.

Mathematical Modelling of Rotary-wing Aircraft

The modern practice of mathematical modelling of aircraft flight behaviour for the study of stability, control and handling qualities is based on the analyses and developments made by those associated with the early days of powered flight, such as Lanchester and Bryan [40, 41]. Contemporary texts, for example Babister and Etkin [42, 43], capture those early efforts and thoroughly describe the kinematic and kinetic principles required to construct a model. The standard form is one that captures the unconstrained 6 degree-of-freedom motion of the vehicle under the influence of externally-applied forces and moments, and given that the basis of the formulation is Newtonian mechanics, the result is a set of 9 linear ordinary differential equations having time as the independent variable, albeit in general with non-linear coefficients. Integration gives angular and translational position and velocity hence trajectory; linearisation allows the study of the stability and control properties of the aircraft. Modelling of rotary-wing aircraft is consistent with this approach and in this regard is no different to other flight vehicles. What sets them apart fundamentally is the complexity introduced by additional degrees of freedom of the rotor blades. The order of the system can be increased further by the need to address other higher order dynamics such as those associated with air mass. The intrinsic dual challenge in rotorcraft flight dynamics modelling therefore is not simply incorporation of these effects, but also the determination of appropriate model reduction to allow interpretation in the familiar context of the 6 degree-of-freedom formulation.

It is instructive to review mathematical modelling of rotorcraft in general, prior to further consideration of its application to the gyroplane. Padfield [44] proposed three 'levels' of simulation complexity which remain applicable to the categorisation of these models. Level one describes a family that represents the rotor as a disc rather than individual blades. Within this family the models may be linear or non-linear, and the dynamic behaviour of the disc in response to inputs may be

regarded as quasi-steady or described by modes of motion. The quasi-steady formulation assumes that the rotor dynamics are fast in relation to the body modes (ie the conventional aircraft flight mechanics modes of motion such as the phugoid, short-period, etc) and hence disc response is instantaneous. Incorporation of rotor modes allows the short-term detail associated with the very fast transients to be included. The order of the model increases with these additional degrees of freedom but it is the case that the rigid-body modes are usually little-changed by these degrees of freedom unless augmentation by means of flight control system gains is large [45]. Level two models introduce a greater degree of physical realism as they represent the rotor as individual, albeit rigid, blades. The disadvantage of this approach is that physical insight is lost for three reasons: the order of the model grows markedly; the equations of motion become periodic, tending to complicate any analysis such as trim and linearisation; and interpretation of rotor behaviour from multiple individual blade response is near-impossible. However the advantages are significant. First, blade flap, lag and feather dynamics are included explicitly; second, the blade can be split into elements allowing complex variation in mass, geometry and aerodynamic properties to be incorporated; third, high-frequency phenomena such as vibration are captured naturally; fourth, fewer assumptions about linearity of behaviour need be made. Blade element aerodynamic loads are calculated from lookup tables of lift and drag represented as functions of angle of attack and Mach number, but the induced velocity experienced by a blade element is inferred from momentum-based models of inflow. Note that such models are also usually the basis for inflow modelling in level one. They can be complex and complicated; quasi-steady or dynamic. Chen [46] presents a seminal overview of inflow modelling in rotorcraft simulation. Despite the comprehensive nature of a Level 2 model one limitation is that aerodynamic interaction such as that between rotors and airframe components is not incorporated in any manner other than empirical. Level 3 however replaces the aerodynamic model with CFD-type flowfield calculations of the environment in a domain around the aircraft, naturally embracing aerodynamic interaction, for example [47]. Elastic representations of the blade

allow structural and aerodynamic behaviour to be coupled, and level 3 models are therefore regarded as comprehensive rotorcraft simulation codes.

Progression from Level 1 to Level 3 is a progression in bandwidth and hence if a problem in rotorcraft flight dynamics can be determined in terms of frequency range, the model description is largely defined. This is only partly true; aircraft stability and control problems are low-frequency in nature which would tend to suggest Level 1 as an appropriate construct. However, Level 1 may fail to capture the degree of non-linearity offered by a Level 2 model, and hence Level 2 may be the option of choice. The model can still be trimmed and linearised (by numerical rather than analytical means) to any lower order for purposes of analysis. Indeed, if the model is to be validated against flight test data then such linearisation may be essential as the validation tools available remain structurally in linearised Level 1 format [48].

Modelling from flight test data using system identification techniques is an important complement to analytical modelling, providing not only the basis for validation of the latter but also as a means of cataloguing actual descriptions of the real aircraft. These modelling tools may be based in time or frequency domains. A thorough review of rotorcraft system identification and parameter estimation by AGARD, including direct comparison of time and frequency domain methods across a number of different aircraft served to benchmark the applicability and capabilities of these analysis tools [49 - 52]. Although time domain approaches have been used in rotorcraft studies [53], Tischler (and others) present a compelling argument for frequency domain analysis where the repeatability and consistency achieved indicates that the approach is robust [48, 54 - 56]. The frequency domain method delivers models classified as two types: parametric, and non-parametric. The non-parametric model is a frequency response, the gain and phase interpreted to provide an impression of the response characteristics; the parametric model seeks to fit a model structure to the frequency domain data. The model structure typically has been the conventional aircraft 6 degree-of-freedom

model, with the clear advantage of familiarity to the flight dynamicist as the coefficients are recognisable as conventional derivatives such as pitch damping M_q, etc. The parameterised 6 degree-of-freedom frequency domain model however comes at a price – being linear it is limited in response amplitude applicability, and the structure limits the bandwidth of the model. Bandwidth can be improved by augmenting the model structure with higher order dynamics terms such as those associated with disc flapping modes, but insight is then lost through complexity and the model remains linear. However, the derivation of rotorcraft mathematical models from flight test data does require due consideration of higher order dynamics in the calculation of the derivatives, otherwise biased estimates will be obtained [49]. Some analyses have identified derivative models of some aspects of these higher order dynamics; the conventional approach to obtaining unbiased 6 degree-of-freedom derivatives is to account for unmodelled high frequency effects by means of time delays.

Mathematical Modelling of Gyroplanes

(i) Nonlinear theoretical model description

The model used in the gyroplane studies examined here straddles the Level 2/3 boundary, depending on the inflow model chosen. At the high end of Level 2 it incorporates the Peters dynamic inflow model for induced velocity [15]; as a low-end Level 3 model it uses a vorticity transport formulation of the flowfield around the aircraft [47] – blades however remain rigid (although of course free to flap), pegging the model as a low-end Level 3 type. It has been in use for a number of years for a variety of helicopter and gyroplane studies [6, 10, 11]. It is a generic model, rendered type-specific by means of an appropriate datafile for a given aircraft. No changes are made to the mathematical representation of the physical behaviour of the aircraft to study the gyroplane. In this respect the only degree of uncertainty regarding the applicability of the model to problems in autorotation is with respect to the dynamic inflow model. However, a recent detailed examination found this element is appropriate for use in autorotation and would require only trivial amendment for certain extreme flight conditions [10, 11].

The model is a generic rotorcraft simulation code, and takes the form

$$\underline{\dot{x}} = f(\underline{x}, \underline{u}) \tag{1}$$

where the state vector $\underline{x}$ contains the airframe translational and angular velocity, blade flap, lag and feather angles and rates for each blade on each rotor, a finite number of induced velocity states for each rotor wake as well as the angular velocity of both rotors, and the engine torques. Elements of the control vector $\underline{u}$ are the four controls, which vary with aircraft type e.g. single main and tail rotor helicopter configurations will have three main rotor controls and one tail rotor control. Blade

attachment is modelled as offset hinges and springs, with a linear lag damper. The aerodynamic and inertial loads are represented by up to 20 elements per blade. Rotor blade aerodynamics are functions of blade section angle of attack and Mach number, derived from 2-D lookup tables. Airframe aerodynamics are functions of angle of attack and sideslip, also derived from 2-D lookup tables. Depending on the number of blades on each rotor, there can be up to 100 non-linear, periodic ordinary differential equations describing the coupled rotor/airframe behaviour. A simple model of the International Standard Atmosphere is used, with provision for variation in sea level temperature and pressure. It is accepted that fuselage blockage effects on the main rotor can be important in autorotation. However aerodynamic interactions, other than between main rotor wake and tailplane, are not included due to lack of appropriate empirical data. It is pertinent to consider that previous validation of the model for gyroplane applications [6] has shown that heave and drag damping derivatives are somewhat in error, which could be an indication of the significance of airframe and rotor interference effects in autorotation.

A complete mathematical description of the model is outside the scope of this Paper. Arguably the most significant element is the rotor model, hence the blade equations of motion, the force and moment expressions, the induced velocity model and the optional full wake model, are summarized below.

<u>Blade motion and hub loads</u>

The blade equations of motion are based on the derivation given elsewhere [57], viz

$$I_{flap}\left(\dot{\omega}_x^{bl} + \omega_y^{bl}\omega_z^{bl}\right) - m_{bl}y_{cg}^{bl}a_z^{hinge} = M_{flap}^{bl}$$

$$I_{pitch}\left(\dot{\omega}_y^{bl} - \omega_x^{bl}\omega_z^{bl}\right) = M_{pitch}^{bl} \qquad (2)$$

$$I_{lag}\left(\dot{\omega}_z^{bl} - \omega_x^{bl}\omega_y^{bl}\right) + m_{bl}y_{cg}^{bl}a_x^{hinge} = M_{lag}^{bl}$$

Expressions for the rotor blade angular velocities $\omega_x^{bl}, \omega_y^{bl}, \omega_z^{bl}$ are derived elsewhere [38]. Hinge acceleration terms a_x^{hinge} and a_z^{hinge} are derived using standard kinematic principles. Note that the applied moment terms M_{flap}^{bl} and M_{lag}^{bl} include spring restraint terms, to be used if appropriate, and the lag degree of freedom embodies a very rudimentary lag damper term.

The rotor forces and moments are given by

$$\underline{X} = T_1^{-1} \sum_{j=1}^{nblades} \left(T_2^{-1} T_3^{-1} \left\{ \sum_{i=1}^{nelem} \underline{X}_{elem} \right\} \right) \tag{3}$$

$$\underline{L} = T_1^{-1} \sum_{j=1}^{nblades} \left(T_2^{-1} \left(-\underline{r}_{hinge} \times \left(T_3^{-1} \left\{ \sum_{i=1}^{nelem} \underline{X}_{elem} \right\} \right) \right) \right) + \left(\underline{r}_{hub} - \underline{r}_{cg} \right) \times \underline{X} \tag{4}$$

where

$$\underline{X}_{elem} = \underline{X}_{elem}^{aero} + \underline{X}_{elem}^{inertial} \tag{5}$$

The matrices T_1, T_2 and T_3 transform quantities from blade element to rotor and non-rotating airframe axes. Development of these equations is given by Houston [3].

Dynamic inflow model

The dynamic inflow representation used is due to Peters, [15]. The basic form of induced velocity at any azimuth and radial station over the rotor is given by

$$v_i(r,\psi) = v_{i0} + \frac{r}{R} v_{1s} sin\psi + \frac{r}{R} v_{1c} cos\psi \tag{6}$$

The induced velocity $v_i(r,\psi)$ appears explicitly in the aerodynamic model, contributing to the blade element angle of attack. The three states v_{i0}, v_{1s} and v_{1c} are calculated from

$$[\boldsymbol{\tau}] \begin{bmatrix} \dot{v}_{i0} \\ \dot{v}_{1s} \\ \dot{v}_{1c} \end{bmatrix}_{wind} = - \begin{bmatrix} v_{i0} \\ v_{1s} \\ v_{1c} \end{bmatrix}_{wind} + [\boldsymbol{L}] \begin{bmatrix} T_{aero} \\ L_{aero} \\ M_{aero} \end{bmatrix}_{wind} \tag{7}$$

where

$$[\boldsymbol{\tau}] = \begin{bmatrix} \frac{4R}{3\pi v_T C_0} & 0 & \frac{-Rtan(\chi/2)}{12 v_m} \\ 0 & \frac{64R}{45\pi v_m(1+cos\chi)} & 0 \\ \frac{5Rtan(\chi/2)}{8 v_T} & 0 & \frac{64Rcos\chi}{45\pi v_m(1+cos\chi)} \end{bmatrix} \tag{8}$$

and

$$[\boldsymbol{L}] = \frac{1}{\rho\pi R^3} \begin{bmatrix} \frac{R}{2 v_T} & 0 & \frac{15\pi tan(\chi/2)}{64 v_m} \\ 0 & \frac{64R}{45\pi v_m(1+cos\chi)} & 0 \\ \frac{15\pi tan(\chi/2)}{64 v_T} & 0 & \frac{-4cos\chi}{v_m(1+cos\chi)} \end{bmatrix} \tag{9}$$

The reader is referred to the original literature [15] for detail and history of the development of these equations.

<u>Vorticity transport wake model</u>

A full description of this model is given elsewhere [47] and only an outline given here. For aeromechanics purposes, a straightforward way of constructing a comprehensive model for the

aerodynamic environment of the rotor is to represent the wake by a time-dependent vorticity distribution in the region of space surrounding the rotor. If ν is the velocity of the flow then the associated vorticity distribution $\omega = \nabla \times \nu$ evolves according to the unsteady vorticity transport equation

$$\frac{\partial}{\partial t}\omega + \nu.\nabla\omega - \omega.\nabla\nu = S(x) \tag{10}$$

This equation can be derived from the Navier-Stokes equation under the assumption of incompressibility and in the limit of vanishing viscosity [47] and shows the rotor wake to arise as a vorticity source S associated with the generation of aerodynamic loads on the rotor blades. The differential form

$$\nabla^2\nu = -\nabla \times \omega \tag{11}$$

of the Biot-Savart law relates the velocity at any point near the rotor to the vorticity distribution in the flow, and allows the geometry and strength of the rotor wake to feed back into the aerodynamic loading and the dynamics of the rotor.

The vorticity transport model developed by Brown [47] employs a direct computational solution of equation (10) to simulate the evolution of the wake of the helicopter. The model is capable of faithfully representing blade-wake interactions, as well as the wake-wake interactions that lead to the growth, coalescence and rupture of vortical structures in the rotor wake, and thus embodies a

high level of physical realism. This model is coupled into the flight mechanics simulation by using the loads generated by the rotor's lifting-line aerodynamic model to construct S in terms of the shed and trailed vorticity from the blades on each rotor. After casting the equations on a structured computational grid surrounding the rotor, equation (11) is solved by cyclic reduction, while equation (10) is marched through time using Toro's Weighted Average Flux algorithm [58].

The principal advantage of this method is that it can deal naturally with interactional aerodynamic phenomena. This means that the induced velocity field on the rotor may be so complex as to defy description by equation (6). However, simple parameter estimation by regression fit using the finite state model structure facilitates interpretation of the vorticity transport model, and allows direct comparisons to be made.

Implementation

The rotor module is called twice in the simulation code, each rotor being discriminated by data that specify its location and orientation on the airframe, and its characteristics in terms of blade mass distribution, hinge offset and restraint, etc. This means that treatment of the tail rotor (helicopter) or propeller (autogyro) is equally comprehensive. Trim and linearisation is performed using the procedure described elsewhere [38].

(ii) Flight Data Analysis and Model Synthesis Using System Identification

The model structure for which coefficients are to be identified, is of conventional state-space form:

$$\dot{\underline{x}} = A\underline{x} + B\underline{u} \tag{12}$$

where

$$A = \begin{bmatrix} X_u & X_v & X_w & X_p & X_q & X_r & X_\phi & X_\theta & X_\psi & X_\Omega \\ Y_u & Y_v & Y_w & Y_p & Y_q & Y_r & Y_\phi & Y_\theta & Y_\psi & Y_\Omega \\ Z_u & Z_v & Z_w & Z_p & Z_q & Z_r & Z_\phi & Z_\theta & Z_\psi & Z_\Omega \\ L_u & L_v & L_w & L_p & L_q & L_r & L_\phi & L_\theta & L_\psi & L_\Omega \\ M_u & M_v & M_w & M_p & M_q & M_r & M_\phi & M_\theta & M_\psi & M_\Omega \\ N_u & N_v & N_w & N_p & N_q & N_r & N_\phi & N_\theta & N_\psi & N_\Omega \\ 0 & 0 & 0 & 1 & 0 & 0 & 0 & 0 & 0 & 0 \\ 0 & 0 & 0 & 0 & 1 & 0 & 0 & 0 & 0 & 0 \\ 0 & 0 & 0 & 0 & 0 & 1 & 0 & 0 & 0 & 0 \\ Q_u & Q_v & Q_w & Q_p & Q_q & Q_r & Q_\phi & Q_\theta & Q_\psi & Q_\Omega \end{bmatrix} \tag{13}$$

$$B = \begin{bmatrix} X_{\eta_{ped}} & X_{\eta_s} & X_{\eta_c} & X_{\eta_{prop}} \\ Y_{\eta_{ped}} & Y_{\eta_s} & Y_{\eta_c} & Y_{\eta_{prop}} \\ Z_{\eta_{ped}} & Z_{\eta_s} & Z_{\eta_c} & Z_{\eta_{prop}} \\ L_{\eta_{ped}} & L_{\eta_s} & L_{\eta_c} & L_{\eta_{prop}} \\ M_{\eta_{ped}} & M_{\eta_s} & M_{\eta_c} & M_{\eta_{prop}} \\ N_{\eta_{ped}} & N_{\eta_s} & N_{\eta_c} & N_{\eta_{prop}} \\ 0 & 0 & 0 & 0 \\ 0 & 0 & 0 & 0 \\ 0 & 0 & 0 & 0 \\ Q_{\eta_{ped}} & Q_{\eta_s} & Q_{\eta_c} & Q_{\eta_{prop}} \end{bmatrix} \tag{14}$$

and

$$\underline{x} = [u\ v\ w\ p\ q\ r\ \phi\ \theta\ \psi\ \Omega]^T, \underline{u} = \left[\eta_{ped}\ \eta_s\ \eta_c\ \eta_{prop}\right]^T \tag{15}$$

This constitutes is the conventional 9 degree-of-freedom rigid-body flight mechanics model, with the important (and unique) addition of the rotorspeed degree of freedom. The rigid body states are taken to be with respect to a mutually orthogonal, right-handed frame of reference whose origin is at the centre of mass. The longitudinal and vertical axes are respectively parallel and normal to the

keel of the aircraft, with the lateral axis to the right completing the set. This is consistent with the theoretical model. Note that some derivatives have values fixed by gravitational or kinematic contributions (such as X_θ or Z_q) or are normally considered zero for physical or other reasons (such as N_ϕ or M_θ). These terms are retained in the notation of the other more-commonly accepted derivatives to indicate they may be free of constraint in the identification process.

The angular quantities in the state vector, and the control position, are all measured directly. The translational velocities u, v and w are obtained from airspeed, sideslip and angle of attack data measured at the nose-mounted boom, as follows.

$$u = u_{probe} - q\left(z_{vane} - z_{cg}\right) + r(y_{vane} - y_{cg})$$

$$v = v_{probe} + p\left(z_{vane} - z_{cg}\right) - r\left(x_{vane} - x_{cg}\right) \tag{16}$$

$$w = w_{probe} - p\left(y_{vane} - y_{cg}\right) + q(x_{vane} - x_{cg})$$

where

$$u_{probe} = \frac{V_f cos\beta_{vane}}{\sqrt{1 + tan^2\alpha_{vane}}};$$

$$v_{probe} = V_f sin\beta_{vane}; \tag{17}$$

$$w_{probe} = u_{probe} tan\alpha_{vane}$$

The time histories of each variable are then converted into frequency domain information using a Discrete Fourier Transform [51], given by

$$X(k\Delta f) = \Delta t \sum_{n=0}^{N-1} x_n e^{-i2\pi(kn)/N}; k = 0,1,2, \dots . N-1 \tag{18}$$

giving real and imaginary parts of X ,

$$Re[X(k\Delta f)] = \Delta t \sum_{n=0}^{N-1} x_n \cos(2\pi(kn)/N)\,; \;\; Im[X(k\Delta f)] = -\Delta t \sum_{n=0}^{N-1} x_n \sin(2\pi(kn)/N) \tag{19}$$

The quality of these frequency domain data can be enhanced by standard processing techniques such as applying overlapped and tapered windows to the data, as recommended by Tischler, [51].

Each degree of freedom can then be treated separately, and formulation as a linear regression problem allows estimation of the coefficients. The state-space description is converted to the frequency domain, i.e.

$$i\omega \underline{x}(\omega) = A\underline{x}(\omega) + B\underline{u}(\omega) \tag{20}$$

Note that this assumes that any process noise is zero. The unknown coefficients of the A and B matrices are determined by solutions of the frequency domain equations

$$-\omega Im\left[\underline{x}(\omega)\right] = A\left(Re\left[\underline{x}(\omega)\right]\right) + B\left(Re\left[\underline{x}(\omega)\right]\right);$$

$$\omega Re\left[\underline{x}(\omega)\right] = A\left(Im\left[\underline{x}(\omega)\right]\right) + B\left(Im\left[\underline{x}(\omega)\right]\right) \tag{21}$$

This solution applies equal weighting to real and imaginary part errors, which is consistent with the standard weighting for system identification on a Bode plot.

Numerical experiments with this method showed that the model structure given by equations (13-15) could be separated into longitudinal and lateral/directional subsets. This is normally not the case with rotorcraft where cross-coupling between degrees of freedom can be strong. Note also that the use of equivalent time or phase delays to mimic higher-order dynamics such as inflow and blade flapping was also found to be unnecessary up to frequencies of about 1Hz. Since this is beyond the frequency range of task-related pilot inputs it can be argued that derivation of models of light gyroplanes from flight test data is possible with the conventional separated model structures for fixed-wing aeroplanes, provided the rotorspeed degree of freedom is included in the longitudinal subset and cross-coupling is limited. Accordingly, re-ordering and partitioning eq. 13-15,

$$\begin{bmatrix} \dot{\underline{x}}_1 \\ \dot{\underline{x}}_2 \end{bmatrix} = \begin{bmatrix} A_{11} & A_{12} \\ A_{21} & A_{22} \end{bmatrix} \begin{bmatrix} \underline{x}_1 \\ \underline{x}_2 \end{bmatrix} + \begin{bmatrix} B_{11} & B_{12} \\ B_{21} & B_{22} \end{bmatrix} \begin{bmatrix} \underline{u}_1 \\ \underline{u}_2 \end{bmatrix} \tag{22}$$

where

$$A_{11} = \begin{bmatrix} X_u & X_w & X_q & X_\theta & X_\Omega \\ Z_u & Z_w & Z_q & Z_\theta & Z_\Omega \\ M_u & M_w & M_q & M_\theta & M_\Omega \\ 0 & 0 & 1 & 0 & 0 \\ Q_u & Q_w & Q_q & Q_\theta & Q_\Omega \end{bmatrix}, B_{11} = \begin{bmatrix} X_{\eta_s} \\ Z_{\eta_s} \\ M_{\eta_s} \\ 0 \\ Q_{\eta_s} \end{bmatrix} \tag{23}$$

and

$$A_{22} = \begin{bmatrix} Y_v & Y_p & Y_\phi & Y_r & 0 \\ L_v & L_p & 0 & L_r & 0 \\ 0 & 1 & 0 & 0 & 0 \\ N_v & N_p & 0 & N_r & 0 \\ 0 & 0 & 0 & 1 & 0 \end{bmatrix}, B_{22} = \begin{bmatrix} Y_{\eta_{ped}} & Y_{\eta_c} \\ L_{\eta_{ped}} & L_{\eta_c} \\ 0 & 0 \\ N_{\eta_{ped}} & N_{\eta_c} \\ 0 & 0 \end{bmatrix} \tag{24}$$

The off-diagonal minors are null. In the frequency domain, the pitching moment equation for example, is then expressed as the two equations

$$-\omega Im[q(\omega)] = M_u Re[u(\omega)] + M_w Re[w(\omega)] + M_q Re[q(\omega)] + M_\theta Re[\theta(\omega)] + M_\Omega Re[\Omega(\omega)]$$

$$+M_{\eta_s} Re[\eta_s(\omega)];$$

$$\omega Re[q(\omega)] = M_u Im[u(\omega)] + M_w Im[w(\omega)] + M_q Im[q(\omega)] + M_\theta Im[\theta(\omega)] + M_\Omega Im[\Omega(\omega)]$$

$$+M_{\eta_s} Im[\eta_s(\omega)] \tag{25}$$

The other degrees of freedom are in a similar form. Linear regression is then used to estimate values of the coefficients in these equations.

Model structure determination is primarily a qualitative, rather than quantitative process although a formalised guide, informed by analysis of flight test data, can be found [48]. The model structure given by equations (23, 24) is generally, for rotorcraft, compromised by lack of cross-coupling and especially higher order dynamics – both of which can produce biased estimate of the derivatives [53]

However, if acceptable, it is attractive due to its simplicity, familiarity and ease of interpretation. Further, since the theoretical model can be reduced readily to a corresponding form, this structure also forms the basis for model validation. However equations (23, 24) define a limited bandwidth and amplitude and therefore any validation of the theoretical model is limited in scope. Similar formal methods for large amplitude manoeuvres do not exist although FAA requirements for simulator model validation do place stringent limits on matching responses in the time domain [59]. The role of unmodelled dynamics in reduced order formulations such as that given by equations (23, 24) is addressed in the Analysis chapter of this Paper.

Analysis

A valid model of a specific aircraft requires both accurate engineering data to define the simulation as a specific aircraft type, as well as appropriate mathematical representation of the physical processes that determine the vehicle's behaviour. Data is obtained by measurement of actual aircraft characteristics such as geometry, mass and inertia, and the aerodynamic properties of rotor blades and airframe. Errors or uncertainty in these data will compromise model fidelity and it is the case that an iterative process, informed by validation against flight test data, is usually necessary to refine the dataset used with the model. Geometric, mass and inertia data for the modelling described here can be found elsewhere [16]; airframe aerodynamic data is summarised in a comprehensive paper [60]; and blade aerodynamic characteristics for the VPM M16 aircraft (Figure 1) which forms the basis of the analysis, was conducted by Westland Helicopters [61]. The Montgomerie-Parsons aircraft (Figure 2) acquired for supplementary studies used blades whose profile was measured as NACA 8H12, for which comprehensive data are available [62] albeit not as a function of Mach number.

Similarly, unmodelled processes can usually be identified from flight test comparisons and changes to the mathematical description of the governing equations implemented to improve fidelity. However, model complexity can obscure the nature of any deficiencies making rectification a time-consuming and even impossible task. A simple model will expose the underlying physical processes, but it must be accepted that absolute accuracy with such a model is unlikely; however it is usually the case that trends can be captured adequately.

For example a simple model of the aircraft in equilibrium flight, straight and level, can be obtained as follows. First, the in-plane forces acting on a blade element can be written as

$$dQ = r(dLsin\phi - dDcos\phi) \tag{26}$$

Assuming that $C_L = a_0 + a_1\phi$, $C_D = \delta$, then integrating along the radius of a blade and setting $Q = 0$ (autorotation), the torque equation is

$$\dot{m}^2 + \frac{2\Omega R}{3}\frac{a_0}{a_1}\dot{m} - \frac{\delta}{2a_1}\left((\Omega R)^2 + V_f^2\right) = 0 \tag{27}$$

where $\dot{m} = w_{hub} - v_{i0}$ is the mass flow through the rotor disc. Since rotorspeed is unknown, solution of this quadratic equation is accomplished iteratively. Confidence in this simple approach is enhanced when the rotorspeed required to converge on a solution for equation (27) is compared with flight test data for both VPM M16 (Figure 3) and Montgomerie-Parsons aircraft (Figure 4).

Since the induced velocity can be approximated [63] by

$$\mathrm{v_{i0}} = \frac{\mathrm{mg}}{2\rho \mathrm{AV_f}} \tag{28}$$

the angle of attack of a simple rotor disc, neglecting flapping, is then

$$\alpha_D = \sin^{-1}\frac{\dot{m}+v_{i0}}{V_f} \tag{29}$$

The corresponding expression that can be used with flight test data is

$$\alpha_D = \theta + \eta_s \tag{30}$$

Figure 5 presents a comparison of the results obtained using VPM M16 flight test data and equation (30), and the simple model given by equation (29). Whilst simple theory is asymptotic to the flight measurements at high speed, the shape of the curve is exaggerated with decreasing airspeed resulting in a mismatch at low speed of the order of a factor of 3. A similar result is obtained with data from the Montgomerie-Parsons aircraft, Figure 6. Similar, although less exaggerated, behaviour has been noted previously with the comprehensive simulation model [6] but has defied explanation. Since combined blade element and disc induced velocity theory is used in the derivation of the comprehensive model also, it is argued that although rudimentary, the simple representation given by equations (27) - (29) is exposing an unmodelled phenomenon at a fundamental level across the

Level 1/2 modelling spectrum. Analysis of these results shows this unmodelled contribution to inflow that can be represented by

$$w_{hub} = 8.0 - 0.16V_f \tag{31}$$

$$w_{hub} = 2.9 - 0.002V_f \tag{32}$$

for VPM M16 and Montgomerie-Parsons aircraft, respectively. This constitutes additional inflow, perhaps the result of upwash across the whole disc occurring as a result of an aerodynamic interaction, analogous to that experienced by high-wing aeroplanes where the wing/fuselage junction generates localised airflow such that dihedral effect is enhanced.

Implementation of these corrections should be treated with caution: no physical modelling is involved, and hence wider applicability is questionable; they are configuration-specific and therefore not generic in nature, although the form is similar for the two aircraft. However there is consistency in the fact that two dissimilar aircraft display similar characteristics, lending credence to the hypothesis that there is common unmodelled physical behaviour. It is important in a model whose fundamental behaviour is governed by nonlinear phenomena that the trim state is captured accurately since trim is the basis for many analyses in flight mechanics, such as linearisation and calculation of response to control inputs – in a nonlinear model the behaviour of forces and moments under perturbation from trim may very well take a different path from two dissimilar trim points.

Results

Equilibrium flight - trim

Numerical experiments show that the additional contribution to inflow postulated in the previous chapter remains unmodelled in the full non-linear simulation, whether the dynamic inflow or vorticity transport wake model is implemented. However, the corresponding adjustment given by equations (31) and (32) become

$$w_{hub} = 6.0 - 0.141V_f \tag{33}$$

$$w_{hub} = 2.0 - 0.017V_f \tag{34}$$

In both cases there is a slightly more pronounced dependency on speed, but the overall correction is less since the effect of blade flapping is accounted for. The trim solutions were then derived using the procedure described by Houston [39]. Figure 7 shows comparison with flight test data for the VPM M16; Figure 8 for the Montgomerie-Parsons aircraft. Only longitudinal components of the trim solutions are shown.

It might be expected that a common physical model, populated separately with configuration-specific data, might render comparable validation results. However, less-good correlation with flight in the case of the VPM M16 simulation tends to indicate that configuration-specific phenomena are lacking in the model as comparison with flight for this aircraft is less good than it is with the Montgomerie-Parsons machine. Equations (33) and (34) indicate it is certainly the case that greater adjustment of inflow is required in the modelling of the former aircraft, further hinting at a greater degree of unmodelled effects being present.

Note the use of the sophisticated wake model, to capture the flowfield around the entire aircraft, offers no benefit in terms of model fidelity; still requires inflow adjustment (equation (33)); and is computationally-demanding. In addition it proved impossible to trim at very low airspeed, although

extrapolation of the pitch attitude result below 40 mph tends to indicate that the inflow adjustment required may not be as pronounced.

If the significant mathematical comprehensiveness and complexity of a full wake code added to a Level 2 model adds little or nothing to validity, the question arises as to what extent complexity is required to capture steady flight behaviour. At the other extreme end of modelling, a very simple, indeed crude, representation of the trim state can be constructed, compared and contrasted with flight, Figures 9 & 10. In addition to equations (27) - (32), the force and moment balance equations are:

$$T = mg = \frac{1}{4}\rho bcR\left\{\Omega R\dot{m}a_1 + \left[\frac{2}{3}(\Omega R)^2 + V_f^2\right]a_0\right\} \tag{35}$$

$$T_{prop} = \frac{1}{2}\rho V_f^2 S_{fus} C_{D_{fus}} + \frac{1}{4}\rho bcV_f\{\Omega R^2\delta - \dot{m}Ra_0\} + T\alpha_D \tag{36}$$

$$Tx_R + T\eta_s z_R + T_{prop}z_{prop} + \frac{1}{4}\rho bcV_f\{\Omega R^2\delta - \dot{m}Ra_0\}z_R = 0 \tag{37}$$

The results for both aircraft simulations are consistent in that common anomalies are present in the comparisons with the corresponding flight test data, exposing some key issues in the modelling of gyroplane trim state. First, since the disc angle of attack is matched accurately to flight by incorporation of equations (31) and (32), the discrepancies in pitch attitude can be attributed to the mismatch in the longitudinal tilt of the rotor hub. This in turn is a consequence of the lack of that contribution to the airframe pitching moment arising from mast and hub drag, which increases with the square of the airspeed and since is located above the centre of mass, requires increased forward tilt of the rotor (pod and tailplane *lift* contributions to the pitching moment tend to cancel each other out). Second, although the rotorspeed is close to the flight values (lying within 20 rpm of measurement) the trend with airspeed is opposite to that obtained in flight. Consideration of equations (27) and (35) shows that the rotorspeed will tend to reduce slightly with increased airspeed, but the influence of blade airfoil section drag coefficient is paramount – increased drag tends to result in reduced rotorspeed. The flight results therefore tend to suggest that blade drag

coefficient reduces with increased airspeed, consistent with reduction in blade section angle of attack and a trend that would require a polynomial rather than constant representation of drag coefficient in the model.

This is indeed the case with the comprehensive model, whose results in Figures 7 and 8 do show the correct trend with airspeed. Further, with comprehensive wind tunnel-derived data for airframe aerodynamics, in particular the pitching moment due to drag-producing components above the centre-of-mass, the longitudinal tilt is properly represented in both cases and hence the pitch attitude trend and amplitude is properly captured.

Small-amplitude perturbed flight – derivatives

Derivatives will only be physically meaningful if the associated model structure accurately captures the bandwidth of the dynamical system. Whilst the objective is to construct models that are of the conventional 6 DOF format (to aid the conventional interpretation of individual derivatives), it is important to confirm that such a structure is appropriate. The issue with rotorcraft, as always, is unmodelled higher order dynamics associated with the actuation system, inflow and blade flapping. Qualitatively, the role of the former two can be discounted: the light gyroplane has a direct-linkage mechanical control system without actuators; inspection of eq. (8) shows that the inflow dynamics, already of high frequency, become faster as the rotorcraft moves into forward flight since $v_T \rightarrow V_f$ and $v_m \rightarrow V_f$; leaving only the flapping dynamics to address. Consideration of these rotor modes is involved and non-trivial whether treated in the rotating and/or non-rotating frames of reference [64], and a further complication, paradoxically, is the simplicity of the two-bladed rotor. The multiblade coordinates β_0, β_{1s} and β_{1c}, represent the tip-path plane of the rotor in the non-rotating frame of reference typically used in the analysis and interpretation of stability and control. However, the behaviour of the two-bladed rotor can only be interpreted in this form if the response is limited

to low frequencies and hence decoupling the rigid-body and rotor flapping modes. The analysis is therefore *de facto* constrained to be that of the classical 6 DOF model structure and the linearisation conducted accordingly. For rotors with more than two blades (rare in contemporary gyroplanes) the rotor flapping modes in the non-rotating frame are generally three oscillations: the coning mode, and the advancing and regressing flapping modes, the latter pair arising from coupled lateral and longitudinal tilting of the rotor disc. A simple and rough estimate of the characteristic equation can be obtained by assuming centrally-hinged blades for a hovering rotor (forward flight is best dealt with numerically, this approach providing a relatively accurate order-of-magnitude assessment of the modal characteristics). The blade flapping equation is

$$\ddot{\beta} + \frac{\rho ac\Omega R^4}{8I_\beta}\dot{\beta} + \Omega^2\beta = \frac{\rho ac\Omega^2 R^4}{8I_\beta}\theta \tag{38}$$

and the individual to multiblade transformation is

$$\beta = \beta_0 + \beta_{1s}sin\psi + \beta_{1c}cos\psi \tag{39}$$

Engineering data are available for the various parameters, and typical rotorspeed has been measured in flight. The result is the following three modes:

$$\lambda_{adv} = -14 \pm 72.3i \tag{40}$$

$$\lambda_{cone} = -14 \pm 34.8i \tag{41}$$

$$\lambda_{reg} = -14 \pm 2.7i \tag{42}$$

All three are widely separated in modulus from typical rigid body modes, suggesting that the conventional 6 DOF model structure is appropriate for analysis. While the model can be linearised readily in a higher order form to incorporate these flapping modes, doing so results in loss of insight into the nature of the aircraft's behaviour as important derivatives such as those dominated by rotor contributions (eg M_q and L_p) tend to lose their conventional interpretation. Further, identification of models including higher-order flapping dynamics from flight-test data is a significant challenge,

especially without knowledge of flapping behaviour. In summary then, linearisation into the conventional quasi-steady 6 DOF form is deemed appropriate for two-bladed or multi-bladed gyroplane rotors.

Testing the robustness of derivative estimates to the frequency range used in the estimation process can serve to highlight if these higher order modes need to be included. Tables 1 and 2 show that for the VPM M16 data, the derivatives are consistent up to 1Hz. Biased estimates of M_q in particular might be expected if flapping dynamics required inclusion in anything other than the quasi-steady form inherent in the 6 DOF model structure. However the data confirms that the 6 DOF structure, augmented with the additional degree of freedom associated with rotorspeed, is appropriate for modelling up to 1 Hz. The theoretical model was linearised to give the same structure.

Results are shown in Figures 11 and 12. Error bounds associated with the estimate of derivatives from flight test data are generally small for the VPM M16, less so for the Montgomerie-Parsons aircraft. This reflects the difficulty with which flight test control inputs could be made on that machine, and the comparisons between theory and flight are consistently less good too. Overall however, there is generally quite good agreement between flight and theory in some of the significant stability and control derivatives; however the derivatives X_u and Z_w highlight a degree of mismatch in key terms that is indicative of either unmodelled dynamics in the theoretical model; or biased derivative estimates in the flight test data. (These two derivatives are key in that they have dominant roles to play in the damping of the phugoid and short-period modes, respectively). Time-domain verification of the estimates verifies the efficacy of the identified model [4]; however such verification is simply a qualitative measure of confidence in the identification and not necessarily that the derivatives are unbiased. For example, the large error bounds associated with X_u are indicative of a significant degree of uncertainty in the estimation of this derivative. Conversely, a degree of suspicion falls on the possibility of excluded phenomena in the theoretical model, since the discrepancy appears generic given that it afflicts both types. The close interaction of the rotor

and propeller is one plausible explanation, but use of the coupled-wake model fails to resolve the discrepancy, Figure 13.

Simple analytical forms of these two derivatives can be constructed [63]. The heave damping Z_w is dominated by the rotor contribution, and is given by

$$Z_w = \frac{2a_1 V_f \rho s A \Omega R}{m(8V_f + a_1 s \Omega R)} \tag{43}$$

which compares favourably with both levels of modelling, Figure 14. False data cannot be the explanation for the mismatch between flight and theory as the distortions in data values required to provide a match are unfeasible – eq. (43) shows for example that the lift-curve slope would have to be reduced by 50%.

The drag damping X_u comprises terms from main rotor, airframe and propeller. Again, using simple expressions [63] it can be written as

$$X_u = X_{u_{rotor}} + X_{u_{fus}} + X_{u_{prop}} \tag{44}$$

with

$$X_{u_{rotor}} = -\frac{1}{4}\rho s A \Omega R \delta / m \tag{45}$$

$$X_{u_{fus}} = -\rho V_f S_{fus} C_{D_{fus}} / m \tag{46}$$

$$X_{u_{prop}} = -\frac{2a_1(v_{i_{prop}} + V_f)\rho s A \Omega R}{m(8(2v_{i_{prop}} + V_f) + a_1 s \Omega R)} \tag{47}$$

(note that the propeller contribution is determined from the derivation given for a rotor Z_w). Figure 15 shows that the propeller contribution dominates X_u, and eq. (47) indicates that there is no scope for adjustment to simple theory or data that would allow a match with the flight test data estimate. As with Z_w, simple theory provides a good approximation (within 20%) of the values obtained by

linearising the comprehensive nonlinear Level 2 model, albeit with a more pronounced variation with speed.

There is a high degree of confidence in flight estimates of the rotor torque derivatives, due to the narrow error bounds and the model compares favourably with the test results, especially in the low to mid-speed range. It is essential to include rotorspeed as a degree of freedom in the modelling of autorotation as it can vary considerably with flight condition; in addition coupling with the conventional body degrees of freedom is not weak [7]. Helicopter rotors, when powered, will still exhibit rotorspeed variations due to the dynamics of the transmission and engines; however for most analyses rotorspeed can be considered fixed at a nominal value due to the efficacy of modern governing systems such as full-authority digital engine controls (FADEC). It is therefore rare to meet the rotor torque derivatives in the literature and analytical forms of the derivatives for powered or unpowered rotors are absent. However simple, approximate analytical expressions for Q_u, Q_w and Q_Ω are easy to derive from eq. (27) and (28), giving:

$$Q_u = \frac{\rho a_1 bcR^2}{4I_\beta}\left\{\frac{\dot{m}T}{\rho A V_f^2} + \frac{\Omega R a_0 T}{3\rho A V_f^2 a_1} - \frac{\delta}{a_1}V_f\right\} \tag{48}$$

$$Q_w = \frac{\rho a_1 bcR^2}{4I_\beta}\left\{2\dot{m} + \frac{2a_0}{3a_1}\Omega R\right\} \tag{49}$$

$$Q_\Omega = \frac{\rho a_1 bcR^2}{4I_\beta}\left\{\frac{2\dot{m}a_0 R}{3a_1} - \Omega R^2\frac{\delta}{a_1}V_f\right\} \tag{50}$$

Figure 16 presents values obtained using these equations for the VPM M16 configuration, compared with results presented previously from the numerically linearised Level 2 model. This shows that these simple derivations encapsulate the fundamental behaviour included in the comprehensive model and therefore their simplicity can be used to expose the core variables that determine derivative values. For example, eq. (50) shows that a drag coefficient that reduces with airspeed will tend to render Q_Ω less positive, matching the flight result shown in Figure 11. Note that this is also consistent with the argument posed in relation to the behaviour of the rotorspeed in equilibrium

flight at the higher speeds, Figure 7. Likewise, eq. (48) explains that the trend with airspeed seen with Q_{u} is due to the dominant effect of the $\frac{1}{V_f^2}$ terms, themselves traced directly to the simple expression for induced velocity, eq. (28). The dynamic inflow model used in the full nonlinear Level 2 formulation has the same intrinsic behaviour as this simple expression, hence the similarity in result. If the induced velocity model falls under suspicion for the mismatch with flight in Q_{u}, then it be might be expected that the vorticity transport wake might improve prediction, but this was found not to be the case.

Response to control inputs – nonlinear Level 2 model

The derivatives summarise the small-amplitude or linearised response of the mathematical model. For all their utility and power they represent a view of the model that is limited in amplitude and frequency. Time response of the full, non-linear individual blade/blade element model from which the derivatives can be extracted, is itself limited in frequency and amplitude to the characteristics of the control input applied, yet is viewed usually by the lay reader as the ultimate test of a mathematical model - if it can predict the response to a control input, it is an accurate representation of flight. It is re-iterated however that because only one or two cases can ever be tested, response to control inputs is part of the validation process, not a validation process in its own right, and the following cases illustrate this. Figure 17 shows comparisons of response to a longitudinal stick input for the VPM M16. The longer-term rotorspeed response, i.e. greater than 10 seconds, is more heavily damped in simulation model than in flight. This is entirely consistent with linearised model validation which revealed that the real aircraft has little drag damping, *Xu*, and consequently little phugoid or long-term damping. The opposite is true with the linearised simulation model. The pitch rate response is simulated fairly well, the only anomalous period in time being around 10 sec, consistent with the mismatch in rotorspeed. However, the off-axis response in roll rate displays behaviour familiar to helicopter flight dynamicists, where the amplitude is reasonably predicted in magnitude, but not in phase. Figures 18, 19 and 20 show the response of the

model configured as the Montgomerie-Parsons aircraft, when compared with flight test data. Three separate control input responses are shown: the first is a BCAR Section T compliance demonstration case, where it is desired to excite the phugoid or low-frequency mode; the second and third are doublet inputs designed to excite only the short-period or higher-frequency mode. In Figure 19 (phugoid response) the model is adequate only for about 5 sec after the input has been made, capturing pretty well the angle of attack, pitch rate and rotorspeed response during this time. From 15 sec onwards, the aperiodic instability that is predicted by the model takes over and it can be seen that all three model responses diverge rapidly, whereas the flight data does not. Figure 19 shows the response to a doublet input, where it is to be expected that the longer-term response is not excited, and this is indeed seen to be the case for both model and flight. Short-period pitch rate response is captured well, the angle of attack less so. Rotorspeed judgment is less easy to make due to the limitations of the sensor, but the model and flight correlate at least in that the magnitude of the rotorspeed response is small. Figure 20 shows a very similar input however, in this case, the longer-term response is quite dissimilar to that shown in the previous figure despite the input being very similar (the nominal airspeed is only 5 mph greater and has no bearing on the dynamic response). In this case both the short-period pitch rate and angle of attack are captured accurately. However there is a longer-term, neutrally-damped oscillation not present in the previous case despite the similarity of pilot control input but which is nonetheless captured accurately by the model, at least in terms of damping and frequency if not phase. While this is of credit to the model, the difference in the long-term response between Figure 19 and 20 is perplexing until one inspects the respective control inputs - note that in the case of Figure 20 the pilot control input varies sinusoidally, driving the oscillation seen in the response, whereas in Figure 19 the control is held rigidly fixed after the doublet input is made. This emphasizes that comparing only the response to control inputs does not constitute model validation in the widest sense, but only narrowly verifies that the model can capture a specific control input response.

The criteria used to assess whether or not the rotorcraft model can adequately simulate the gyroplane are necessarily subjective, relying on engineering judgement since there are no formal criteria for gyroplane simulation. However, comparisons with FAA Level D simulator requirements for helicopters, [59], can be instructive. They are expressed in terms of trim and time response comparisons, and the model generally satisfies the requirements for control position prediction to be within 5%, and attitude to be within 1.5 deg. Primary axis time responses would fall within acceptable envelopes, although the cross-coupling would not. The criteria for rotorspeed simulation in autorotation is not pertinent to the gyroplane.

Discussion

The autogyro configuration requires no special or additional mathematical modelling treatment to that of rotorcraft in general. Well-understood and widely-used approaches to the problem, across the various Levels of modelling, generate models of fidelity comparable to that achievable for helicopters. Synthesis of validation examples from flight test data follow the methods and pattern that have become the standard for the helicopter industry. However, the generation of a vehicle dataset, necessary to characterise a generic model as a specific machine, is more of a challenge due to the limited resources available to the gyroplane community. Mass, inertia and geometric properties can be determined readily from simple measurements, but the aerodynamic properties of blades and in particular the airframe, are impossible to determine without a comprehensive wind tunnel programme. The modelling of rotorspeed behaviour for example is sensitive to the presence of geometric blade pitch, including any twist that may be present, and in particular the coefficient of lift at zero angle of incidence such as found with non-symmetric sections. The importance of blade section drag is paramount, having a direct impact on rotorspeed in equilibrium flight as well as the damping of the rotorspeed mode. The literature is relatively sparse on these matters and for specific sections, is largely absent in the context of compressibility effects. Such uncertainty in the data that defines the model as a specific type can obviously compromise fidelity, but it can also mask the nature of deficiencies associated with any unmodelled physical phenomena which are arguably more important to distil given their generic nature.

The compact, close-coupled layout of most light gyroplanes may in fact be the source of those modelling discrepancies whose source can be attributed to unmodelled behaviour, eg the inflow adjustment required to match rotor disc angle of attack and hence pitch attitude, with flight measurements. Inclusion of the aerodynamic interaction of rotor and propeller by means of a comprehensive wake code fails to address this issue, suggesting a dependency on the effect of the airframe on the aerodynamic environment. This is impossible to address in flight mechanics

modelling, even at Level 3, and so empirical corrections may be the only way forward. Further challenge to the full and complete understanding of gyroplane flight mechanics is encapsulated in the mismatch of certain key derivatives, although this too may be associated with the same, or similar, unmodelled effects. For example, since the drag damping X_u is dominated by the propeller contribution, the pusher layout of the aircraft might suggest a considerable blockage or interaction effect, reducing the contribution of this component to the derivative. The simple expression given in eq. (47) does indicate suggest a reduction in the propeller contribution to X_u if airframe blockage reduces the effect of airspeed on this term. The nature and role of unmodelled effects requires further and wider testing with other aircraft configurations to challenge these results.

The humble stability and control derivative, normally considered *passé* in a contemporary context other than for educational purposes, can serve important roles as evidenced here. First, in analytical form it can focus on dominant or first order contributions to a particular physical behaviour; second, it can help to identify parameter values requiring adjustment; finally, the simple analytical forms examined for the gyroplane are good estimates to those extracted by a numerical linearisation process from the full non-linear model, suggesting that good-quality models can be obtained from simple, elementary theory. Since the rudimentary equilibrium equations, if equipped with appropriate data, give acceptable trim solutions as well, it could be argued that linearised Level 1 modelling is adequate for the simulation of light gyroplanes. However, modelling of both Q_Ω and rotorspeed in equilibrium flight suggests that detailed high-quality knowledge of blade element drag characteristics be known; the easiest way to integrate such data is by means of a blade element model, itself easily implemented via individual blade simulation, ie a Level 2 formulation. This is then consistent with contemporary helicopter flight simulation modelling.

It is normal in the study of rotorcraft flight mechanics to expand the comprehensiveness and complexity of mathematical models to improve predictive ability [65 ,66]. However inclusion of a code to capture the rotor/propeller interactions in the flowfield surrounding the aircraft fails to offer

any advantage over the dynamic inflow model in respect of trim, and dynamic stability (as expressed by linearised derivatives). This is consistent with helicopter experience of the wake code [66] and suggests, by a process of elimination common to flight dynamic analyses, that the sources of unmodelled physical behaviour lie elsewhere, such as aerodynamic interaction with the airframe. Level 2+, ie with a comprehensive wake code, therefore appears to offer little benefit in terms of predictive ability. However, validation efforts have focussed on benign areas of the flight envelope in terms of magnitude and frequency. A wider application of flight mechanics modelling requires Level 2 or Level 2+ to address strong nonlinearity such as blade stall and compressibility, and operation of airframe components at large angles of attack and sideslip.

Conclusions

The generic mathematical modelling of light gyroplane flight mechanics presents no difficulty for contemporary approaches in rotorcraft simulation. However, aspects unique to the gyroplane require accurate data. Specifically, the rotorspeed degree of freedom is sensitive to the blade airfoil section drag data, and requires an individual blade/blade element (Level 2) formulation if both gross behaviour and subtleties are to be captured accurately. Similarly, static stability with respect to airspeed is sensitive to those airframe pitching moment characteristics associated with upper airframe drag, rather than the lift contributions from pod and tailplane. Unmodelled phenomena appear to pose questions in relation to their impact on the angle of attack of the rotor disc, a feature that appears type-specific but can be resolved by means of empirical correction. While simple representations of trim and stability derivatives offer clear insight into the behaviour of high-level modelling, they also can adequately represent flight behaviour in a benign part of the flight envelope (straight and level flight). The use of a wake code coupling the aerodynamic interaction of main rotor and propeller offers little benefit over a finite-state dynamic inflow model that treats the two rotors in isolation. It is concluded therefore that unmodelled behaviour described needs to be challenged and tested by further study, but that the focus, by a process of elimination, should be on the effect of the airframe on aerodynamic environment surrounding the aircraft.

References

[1] Brotherhood, P., 'Stability and Control of the Wallis W117 Autogyro,' Royal Aircraft Establishment Technical Memorandum TM Aero. 1461, 1972.

[2] Arnold, U. T. P., 'Untersuchungen zur Flugmechanik eines Tragschraubers,' Technische Universitat Braunschweig Diplomarbeit 88-5D, March 1988.

[3] Houston, S., 'Longitudinal Stability of Gyroplanes'. The Aeronautical Journal Vol. 100 No. 991, pp. 1-6 (1996)

[4] Houston, S., 'Identification of Autogyro Longitudinal Stability and Control Characteristics'. AIAA Journal of Guidance, Control and Dynamics Vol. 21 No. 3, pp. 391-399 (1998)

[5] Houston S. S., 'Identification of Gyroplane Lateral/Directional Stability and Control Characteristics from Flight Test'. Proc. Inst. Mech. Engrs, Part G, Vol. 212 No. G4, pp. 271-285 (1998)

[6] Houston, S. S., 'Validation of a Rotorcraft Mathematical Model for Autogyro Simulation'. AIAA Journal of Aircraft, Vol. 37 No. 3, pp. 203-209 (2000)

[7] Houston S. S., 'Analysis of Rotorcraft Flight Dynamics in Autorotation'. AIAA Journal of Guidance, Control and Dynamics, Vol. 25 No. 1, pp.33-39 (2002).

[8] Houston S. S., 'Modeling and Analysis of Helicopter Flight Mechanics in Autorotation'. AIAA Journal of Aircraft, Vol. 40 No. 4, pp. 675-682 (2003).

[9] Thomson D. G., Houston S. S., 'Application of Parameter Estimation to Improved Autogyro Simulation Model Fidelity,' AIAA Journal of Aircraft Vol.42 No.1, pp. 33-40 (2005)

[10] Murakami Y., Houston S. S., 'Dynamic Inflow Modelling for Autorotating Rotors,' The Aeronautical Journal Vol. 112 No. 1127, pp. 47-53 (2008)

[11] Murakami Y., Houston S. S., 'Correction of the Definition of Mass-Flow Parameter in Dynamic Inflow Modelling,' Proc. Inst. Mech. Engrs, Part G Vol. 223, pp. 1037-1040 (2009)

[12] Houston S. S., 'Light Gyroplane Empennage Design Considerations,' The Aeronautical Journal Vol. 115 No. 1170, pp. 47-53 (2011)

[13] Houston S. S., Brown R. E., 'Rotor Wake Modeling for Simulation of Helicopter Flight Mechanics in Autorotation,' AIAA Journal of Aircraft Vol. 40 No. 5, pp. 938-945 (2003).

[14] Houston S. S., Thomson D. G., 'Calculation of Rotorcraft Inflow Coefficients Using Blade Flapping Measurements,' AIAA Journal of Aircraft Vol.46 No.5, pp. 1569-1576 (2009)

[15] Peters, D. A., HaQuang, N., 'Dynamic Inflow for Practical Applications,' *Journal of the American Helicopter Society*, Vol. 33, No. 4, 1988, pp. 64-68.

[16] CAA Final Report

[17] Shippen, J., 'Data Acquisition and Analysis of Service Loads in a Light Weight Autogyro,' Proceedings of 52 Annual Forum of the American Helicopter Society, June 1996.

[18] Shippen, J., 'Measurement of Autogyro Control Forces,' Proceedings of the I.Mech.E Part G. Journal of Aerospace Engineering, Vol. 212, No. 1, pp 57 – 60, 1998.

[19] Lopez-Diez, J., Cuerno-Rejado, C., Lopez-Ruiz, J.L., 'Directional Control of a Nonrudder Autogiro-Landing Manoeuvre of the C-30,' Proceedings of the 24th European Rotorcraft Forum, pp. FM11.1 – FM11.9, September 1998

[20] Lopez-Diez, J., Cuerno-Rejado, C., Lopez-Ruiz, J.L., 'Study of Competitive Missions for Autogyros,' Proceedings of the 25th European Rotorcraft Forum, September 1999.

[21] Rapp, H., Wedemeyer, P., Teuber, C., 'Measurement of in-Flight Rotor Blade Loads of an Autogyro'. Proceedings of the 26th European Rotorcraft Forum, pp 101.1 – 101.8, September 2000.

[22] Wang, H-J., Gao, Z., 'Aerodynamic Virtue and Steady Rotary Speed of Autorotating Rotor,' Acta Aeronautica et Astronautica Sinica, Vol. 22, No. 4, pp. 337 – 339, July 2001.

[23] Kalmykov, A.A., 'Realizable Combinations of Gyroplane Main Rotor Overload and Starting,' Aviatsionnaya Tekhnika, No. 2, pp 6 – 10, April – June 2004.

[24] McCormick, B.W., 'A Numerical Analysis of Autogyro Performance,' Proceedings of the Biennial International Powered Lift Conference and Exhibit, AIAA Paper No. AIAA-2002-5950, November 2002.

[25] Traum, M.J., Carter, R.G., 'Pitch Control Benefits of Elevators for Autogyros in Low-Speed Forward Flight,' 43rd AIAA Aerospace Sciences Meeting and Exhibit, AIAA Paper No. AIAA 2005 – 26, January 2005.

[26] Li, Y., DeLaurentis, D, Mavris, D., 'Advanced Rotorcraft Concept Development and Selection Using a Probabilistic Methodology,' Proceedings of the 3rd Annual AIAA Aviation Technology, Integration, and Operations Forum, Paper No. AIAA 2003-6759, November 2003.

[27] Ahn, B-H, DeLaurentis, D., Mavris, D.N., 'Advanced Personal Air Vehicle Concept Development Using Powered Rotor and Autogyro Configurations,' Proceedings of the 2nd Annual AIAA Aviation Technology, Integration, and Operations Forum, October 2002.

[28] Jensen, D.I., 'Un-manned Autogyro for Cinematography and Reconnaissance,' Proceedings of Aircraft, Technology Integration and Operations Forum, AIAA Paper No. AIAA-2001-5228, October 2001.

[29] Lopez, C.A., Wells, V.L., 'Dynamics and Stability of an Autorotating Rotor/Wing Unmanned Aircraft' AIAA Journal of Guidance, Control, and Dynamics, Vol. 27, Part 2, pp 258 – 270, 2004.

[30] Somov, Y.I., Polyntsev, O.Y., 'Nonlinear Dynamics and Robust Control of a Windmilling Gyroplane Rotor,' Proceedings of the International Conference on Physics and Control, August 2003.

[31] Somov, Y.I., Polyntsev, O.Y., 'Nonlinear Dynamics and Robust Control of a Gyroplane Rotor,' Proceedings of the IFAC Congress, 2005.

[32] Carter, J. Jr., 'CarterCopter – A High Technology Gyroplane,' Proceedings of the Vertical Lift Aircraft Design Conference, Jan. 2000.

[33] Whitney, M.J., Shah, A.H., 'Dynamic Analysis of the Hawk 4 Rotor Blade,' Proceedings of the 43rd AIAA/ASME/ASCE/AHS/ASC Structures, Structural Dynamics and Materials Conference, Paper No. AIAA-2002-1605, April 2002. August 2010

[34] Groen, D., 'Gyroplane Technology,' Proceedings of the International Air and Space Symposium and Exposition: The Next 100 Years, Paper No. AIAA-2003-2519, July 2003.

[35] Gibbings, D., 'The Fairey Rotodyne: Technology Before Its Time?,' The Aeronautical Journal, Vol. 108, No. 1089, pp. 565 – 574, 2004.

[36] Leishman, J.G., 'Development of the Autogiro: A Technical Perspective,' AIAA Journal of Aircraft, Vol. 41, No. 4, July-August 2004.

[37] Harris, F. D., 'Introduction to Autogyros, Helicopters and other V/STOL Aircraft – Volume 1: Overview and Autogyros,' NASA/SP–2011-215959, May 2011.

[38] Houston, S. S., 'Validation of a Non-linear Individual Blade Rotorcraft Flight Dynamics Model Using a Perturbation Method,' *The Aeronautical Journal*, Vol. 98, No. 977, 1994, pp. 260-266.

[39] Houston, S. S., 'Validation of a Blade-Element Helicopter Model for Large-Amplitude Manoeuvres,' *The Aeronautical Journal*, Vol. 101, No. 1001, 1997, pp. 1-7.

[40] Lanchester, F. W., '*Aerodonetics*,' A. constable & Co., Ltd., London, 1908.

[41] Bryan, G. H., '*Stability in Aviation*,' Macmillan Co., London, 1911.

[42] Babister, A. W., '*Aircraft Dynamic Stability and Response*,' Pergamon Press, Oxford, 1980.

[43] Etkin, B., '*Dynamics of Atmospheric Flight*,' John Wiley & Sons, Inc., Toronto, 1972.

[44] Padfield, G. D., '*Helicopter Flight Dynamics*,' Blackwell Science, Oxford, 1996, p. 90.

[45] *J. Howitt, J., Howell, S. E., McCallum, A. T., '*Experimental Evaluation of Flight Control System Designs Exploiting Rotor State Feedback,' 57th Annual Forum of the American Helicopter Society, Washington DC, May 2001.

[46] Chen, R.T.N., 'A Survey of Nonuniform Inflow Models for Rotorcraft Flight Dynamics and Control Applications,' *Vertica*, Vol. 14, No. 2, 1990, pp. 147-184.

[47] Brown, R. E., 'Rotor Wake Modeling for Flight Dynamic Simulation of Helicopters,' *AIAA Journal*, Vol. 38, No. 1, January 2000, pp. 57-63.

[48] Tischler, M. B., Remple, R. K., 'Aircraft and Rotorcraft System Identification – Engineering Methods with Flight Test Examples,' AIAA Education Series, Reston, 2006, pp. 1-23.

[49] Murray-Smith, D. J., 'Modelling Aspects and Robustness Issues in Rotorcraft System Identification,' AGARD LS178, pp. 6-1 to 6-4, October 1991.

[50] Kaletka, J., 'Instrumentation and Data Processing,' AGARD LS178, pp. 3-1 to 3-18, October 1991.

[51] Tischler, M. B., 'Identification Techniques, Frequency Domain Methods,' AGARD LS178, pp. 6-1 to 6-4, October 1991.

[52] Padfield, G. D., 'SA330 Puma Identification Results,' AGARD LS178, pp. 10-1 to 10-38, October 1991.

[53] de Leeuw, J. H., 'Identification Techniques, Model Structure and Time Domain Methods,' AGARD LS178, pp. 5-1 to 5-9, October 1991.

[54] Fu, K.-H., Marchand, M., 'Helicopter System Identification in the Frequency Domain,' *Proceedings of the 9th. European Rotorcraft Forum,* Sept. 1983.

[55] Tischler, M. B., et al, 'Demonstration of Frequency-Sweep Testing Technique using a Bell 214-ST Helicopter,' NASA TM-89422, April 1987.

[56] Tischler, M. B., 'Frequency-Response Identification of XV-15 Tilt-Rotor Aircraft Dynamics,' NASA TM-89428, May 1987.

[57] Gaonkar, G. H., Peters, D. A., 'A Review of Dynamic Inflow Modeling for Rotorcraft Flight Dynamics,' *Vertica*, Vol. 12, No. 3, 1988, pp. 213-242.

[58] Toro, E. F., 'A Weighted Average Flux Method for Hyperbolic Conservation Laws,' *Proceedings of the Royal Society of London, Series A: Mathematical and Physical Sciences*, Vol. 423, No. 1864, 1989, pp. 401-418.

[59] Anon, "Helicopter Simulator Qualification", US Dept. of Transport Federal Aviation Administration Advisory Circular AC 120-63, Nov. 1994.

[60] Coton, F., Smrcek, L., Patek, Z., "Aerodynamic Characteristics of a Gyroplane Configuration", *AIAA Journal of Aircraft*, Vol. 35, No. 2, 1998, pp.274-279.

[61] Brocklehurst, A., 'An Assessment of the Aerodynamic Performance of an Aerofoil Section from an Autogyro Blade and Comparison with NACA 8-H-12,' GKN Westland Helicopters Technical Note GEN/295, February 1997.

[62] Schaefer, R.F., Smith, H.A., 'Aerodynamic Characteristics of the NACA 8-H-12 Airfoil Section at Six Reynolds Numbers,' NACA Tech. Note 1998, December 1949.

[63] Bramwell, A. R. S., 'Helicopter Dynamics,' Arnold, London, 1976, pp. 186-209.

[64] Johnson, W., '*Helicopter Theory*,' Dover Publications, Inc, New York, 1994, pp. 601-622.

[65] Turnour, S. R., Celi, R., 'Modeling of Flexible Rotor Blades for Helicopter Flight Dynamics Applications,' *Journal of the American Helicopter Society*, Vol. 41, No. 1, 1996, pp. 52-61.

[66] Brown R. E.**,** Houston S. S., 'Comparison of Induced Velocity Models for Helicopter Flight Mechanics,' *AIAA Journal of Aircraft,* Vol. 37, No. 4, 2000, pp. 938-945.

Figure 1: The VPM-M16 Gyroplane

Figure 2: The Montgomerie-Parsons Gyroplane

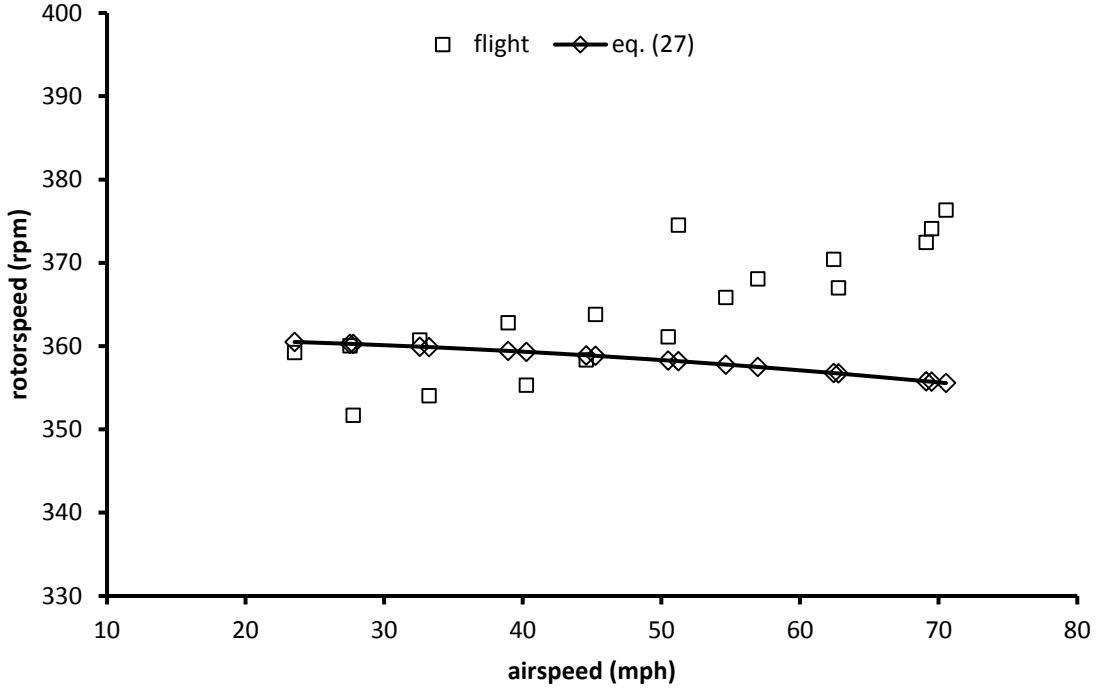

Figure 3: Rotorspeed Comparison – VPM M16 Flight & Simple Theory

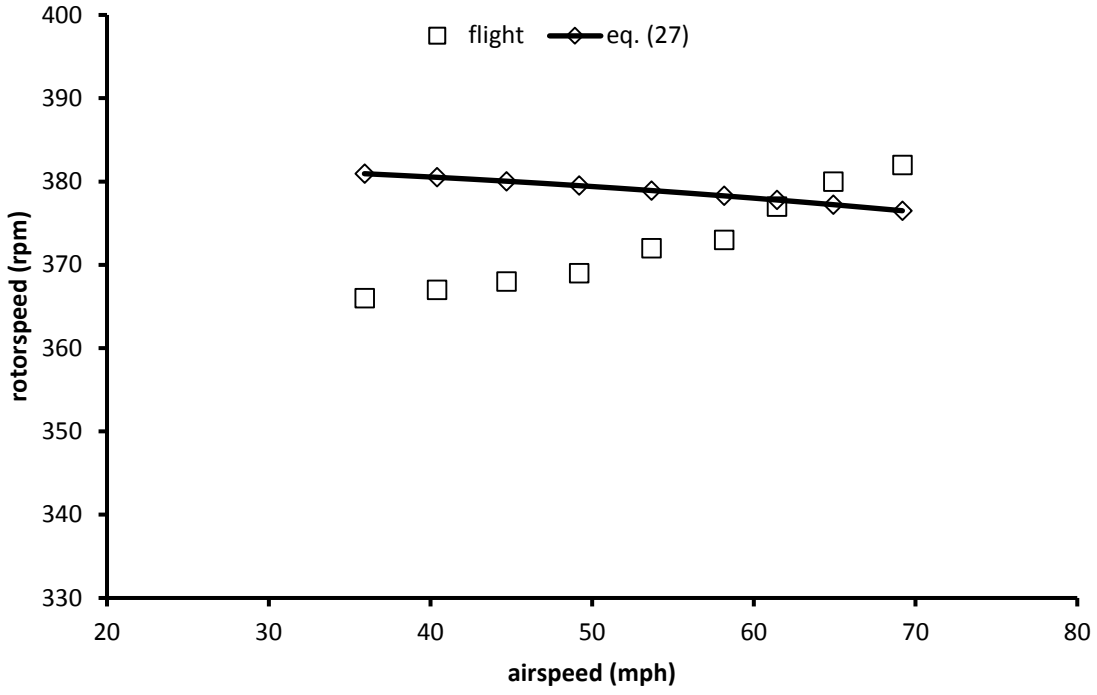

Figure 4: Rotorspeed Comparison – Montgomerie-Parsons Flight & Simple Theory

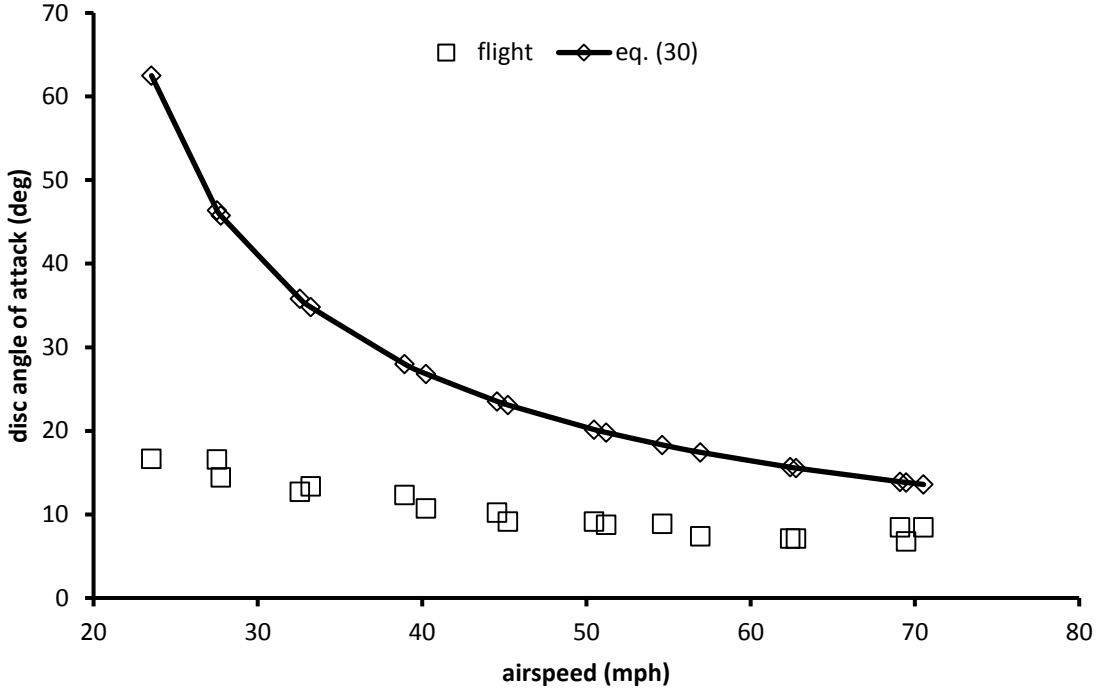

Figure 5: Rotor Disc Angle of Attack Comparison – VPM M16 Flight & Simple Theory

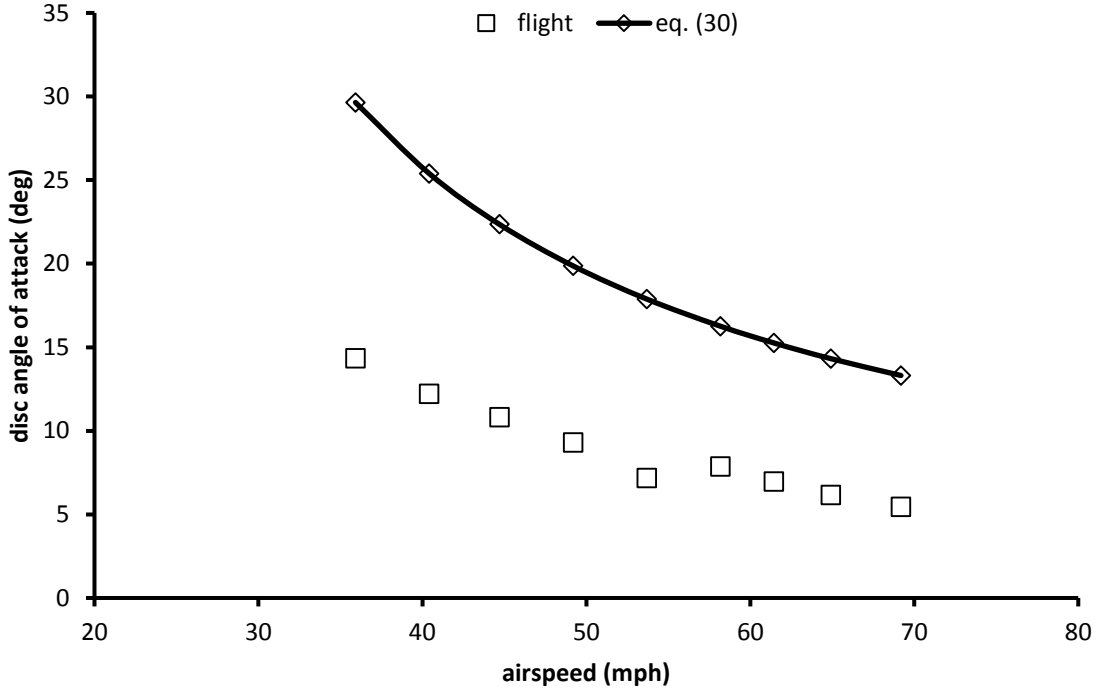

Figure 6: Rotor Disc Angle of Attack Comparison – Montgomerie-Parsons Flight & Simple Theory

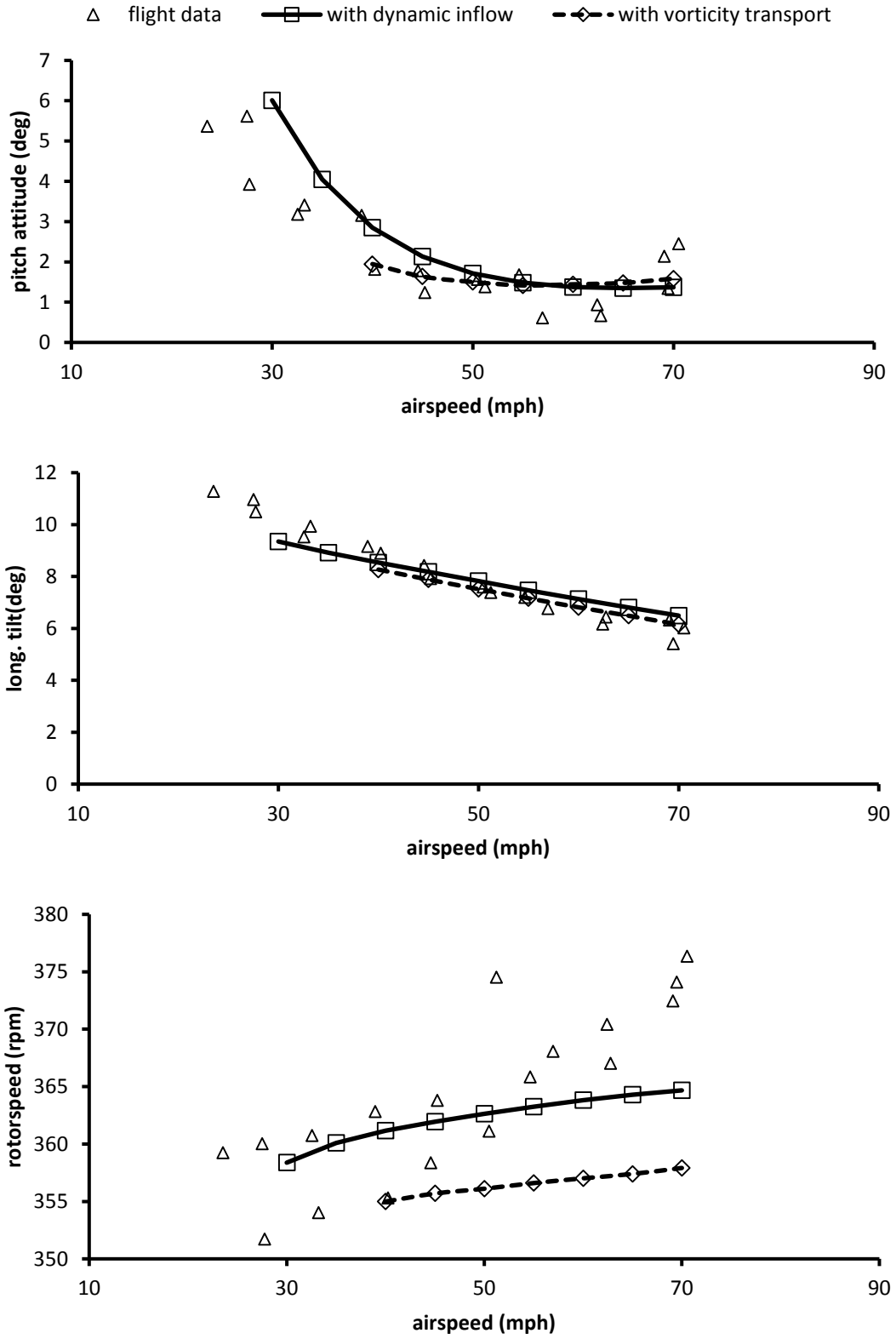

Figure 7: Trim Comparisons, VPM M16

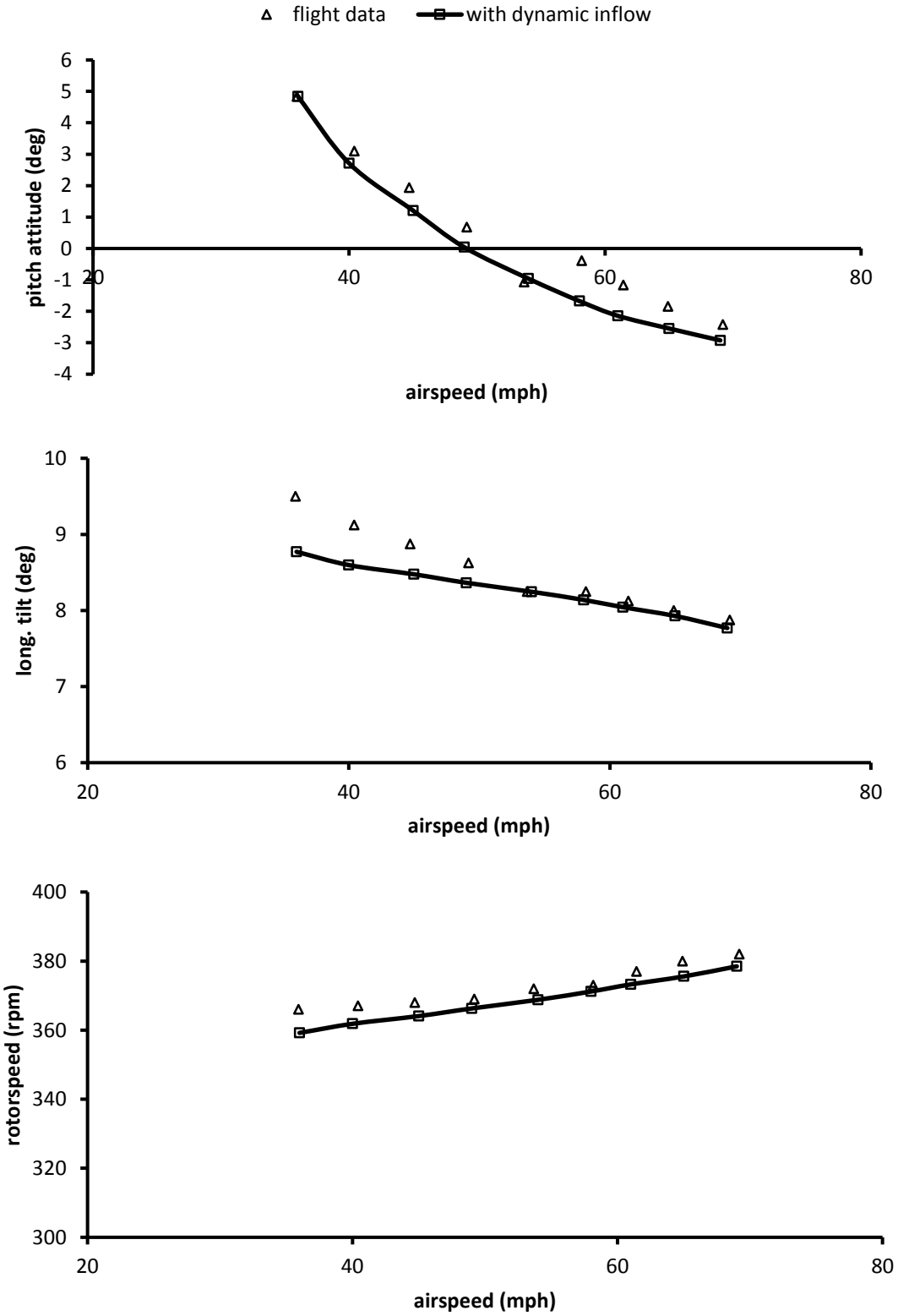

Figure 8: Trim Comparisons, Montgomerie-Parsons

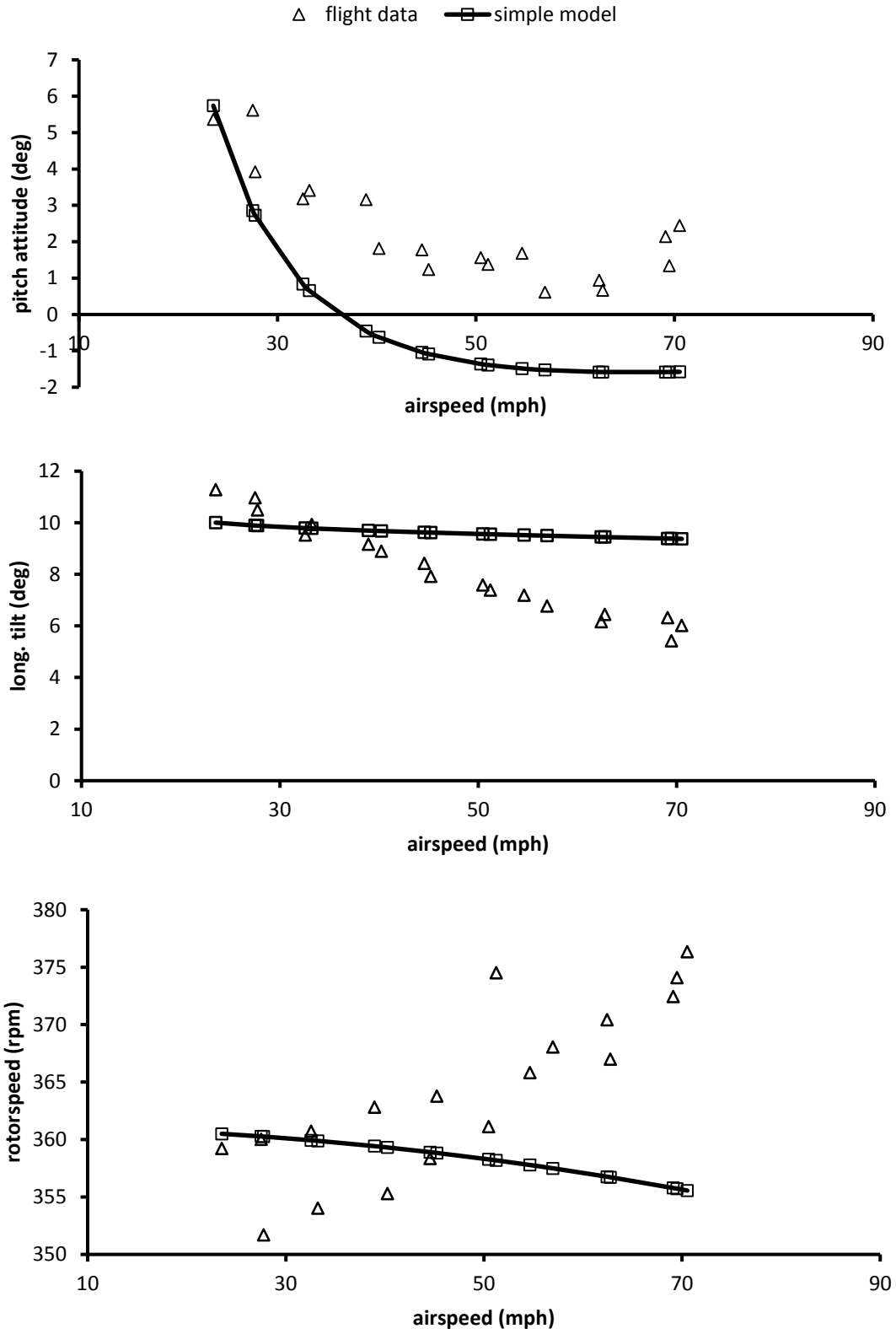

Figure 9: Trim Comparisons, VPM M16 – Simple Model

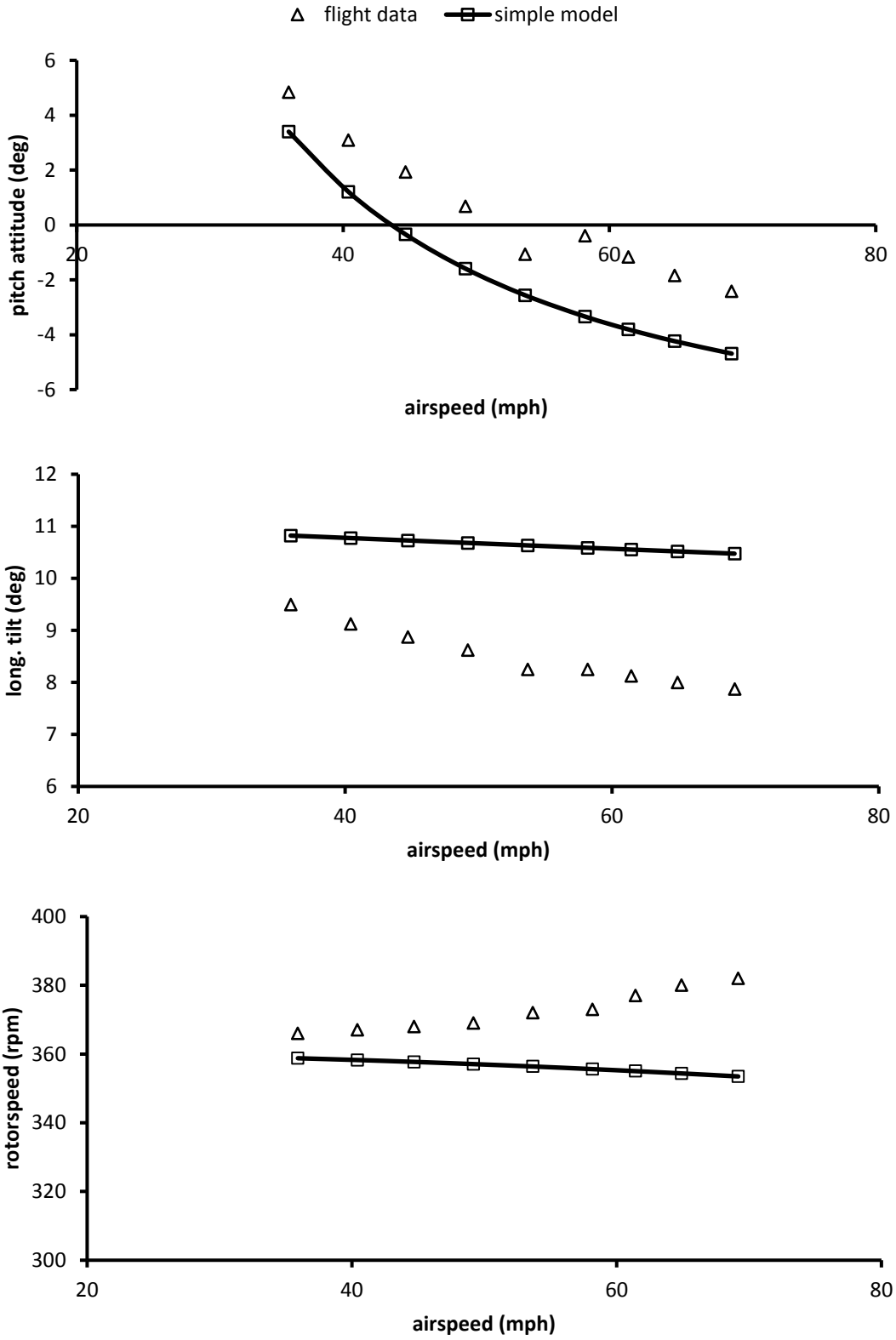

Figure 10: Trim Comparisons, Montgomerie-Parsons – Simple Model

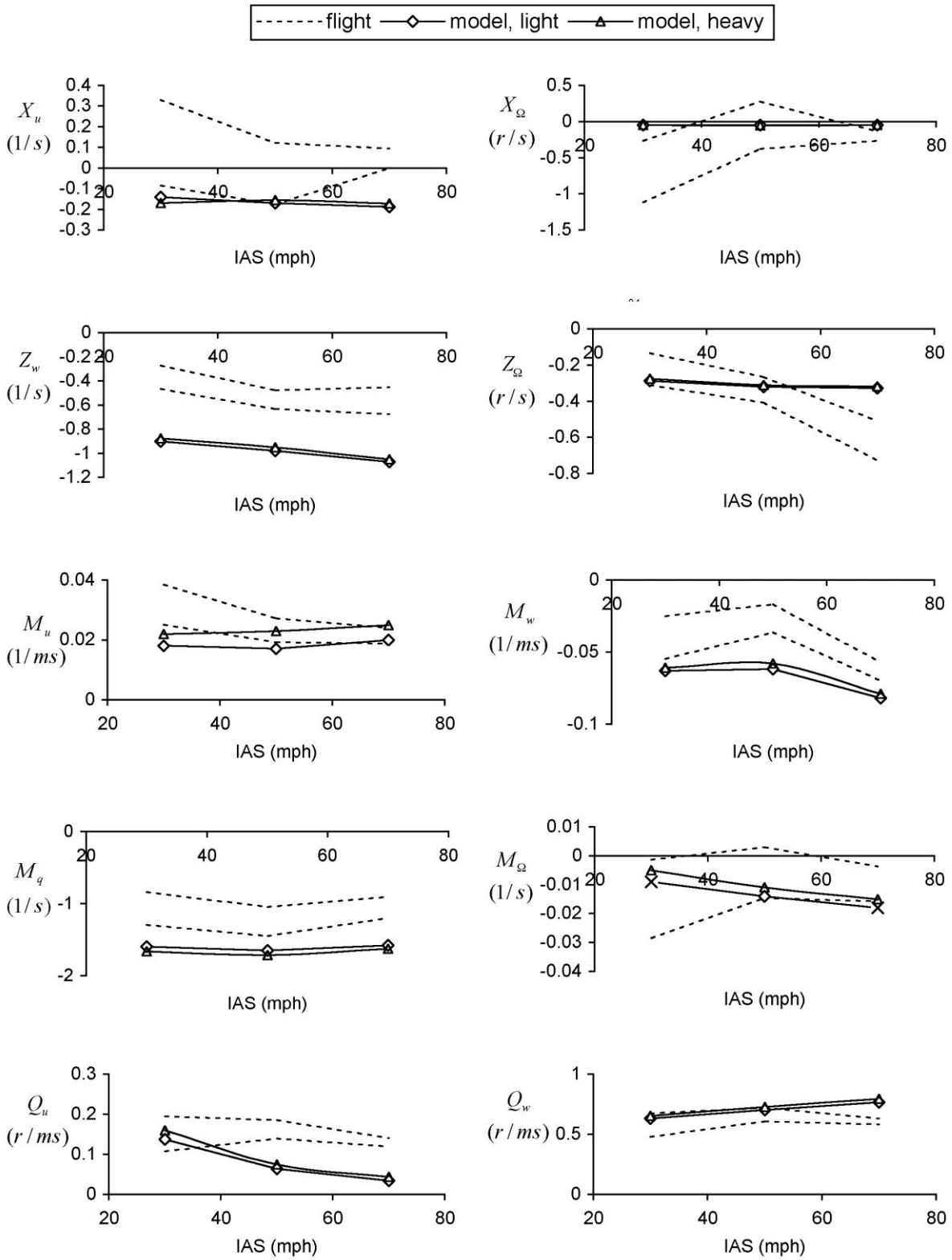

Figure 11: Comparison of Flight and Model Data, Derivatives, VPM M16

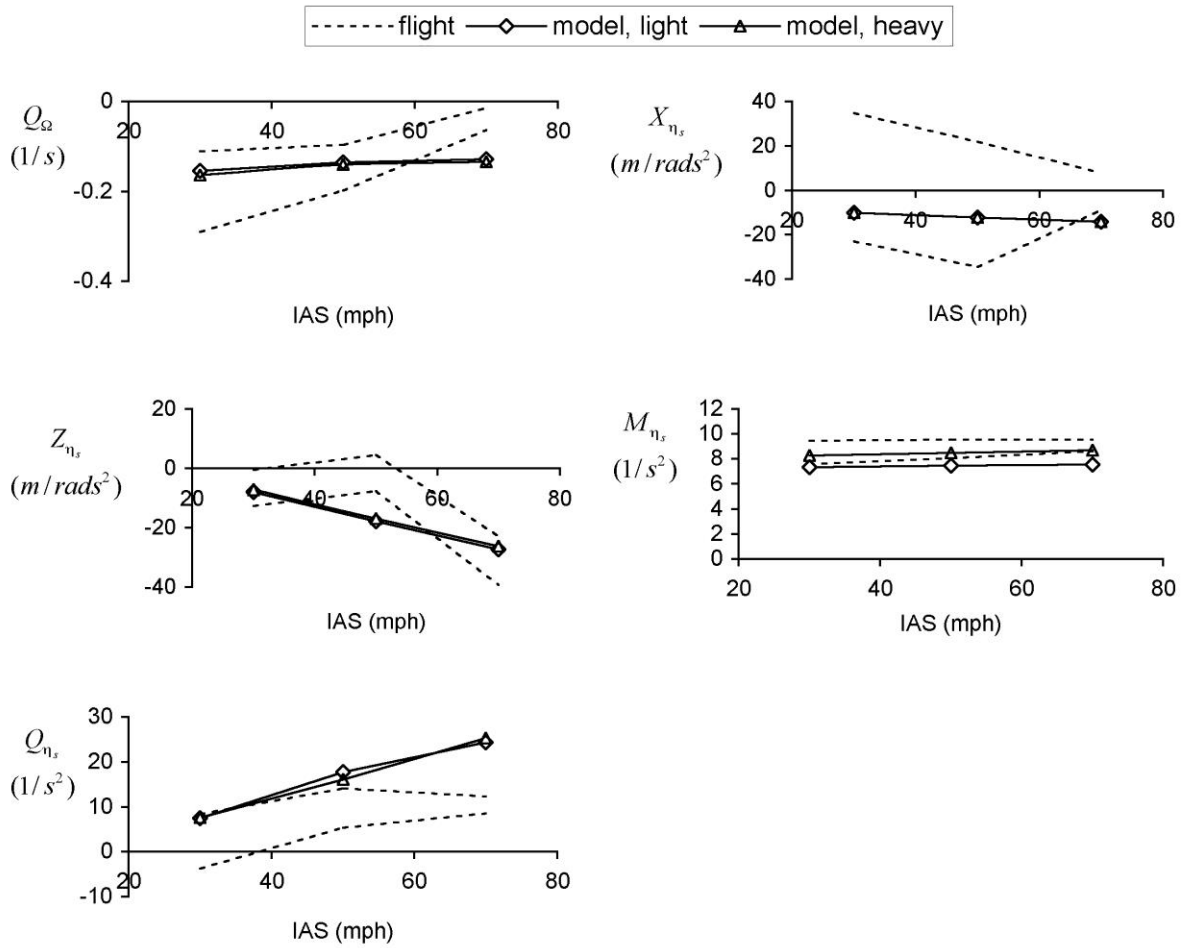

Figure 11: Comparison of Flight and Model Data, Derivatives, VPM M16 (concluded)

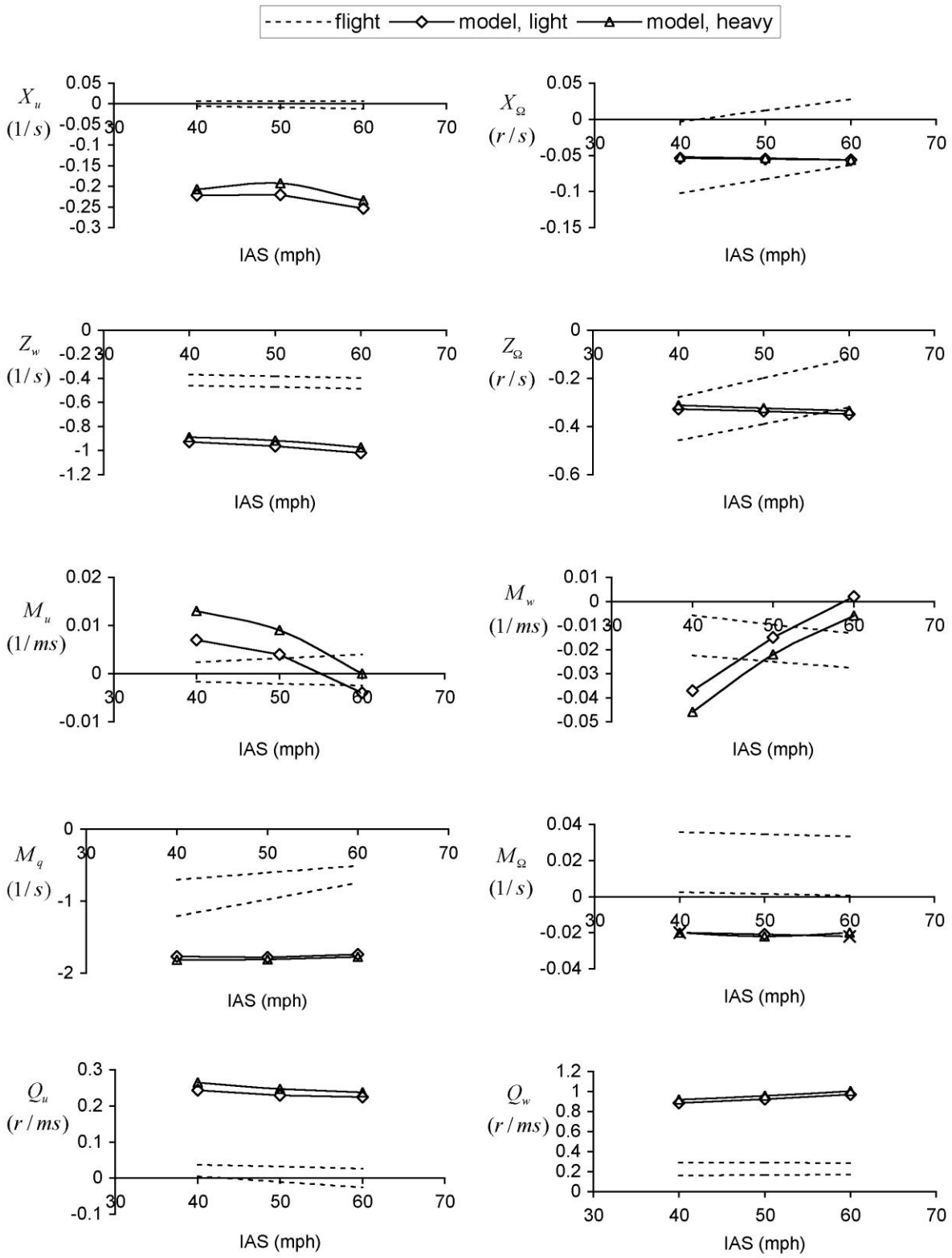

Figure 12: Comparison of Flight and Model Data, Derivatives, Montgomerie

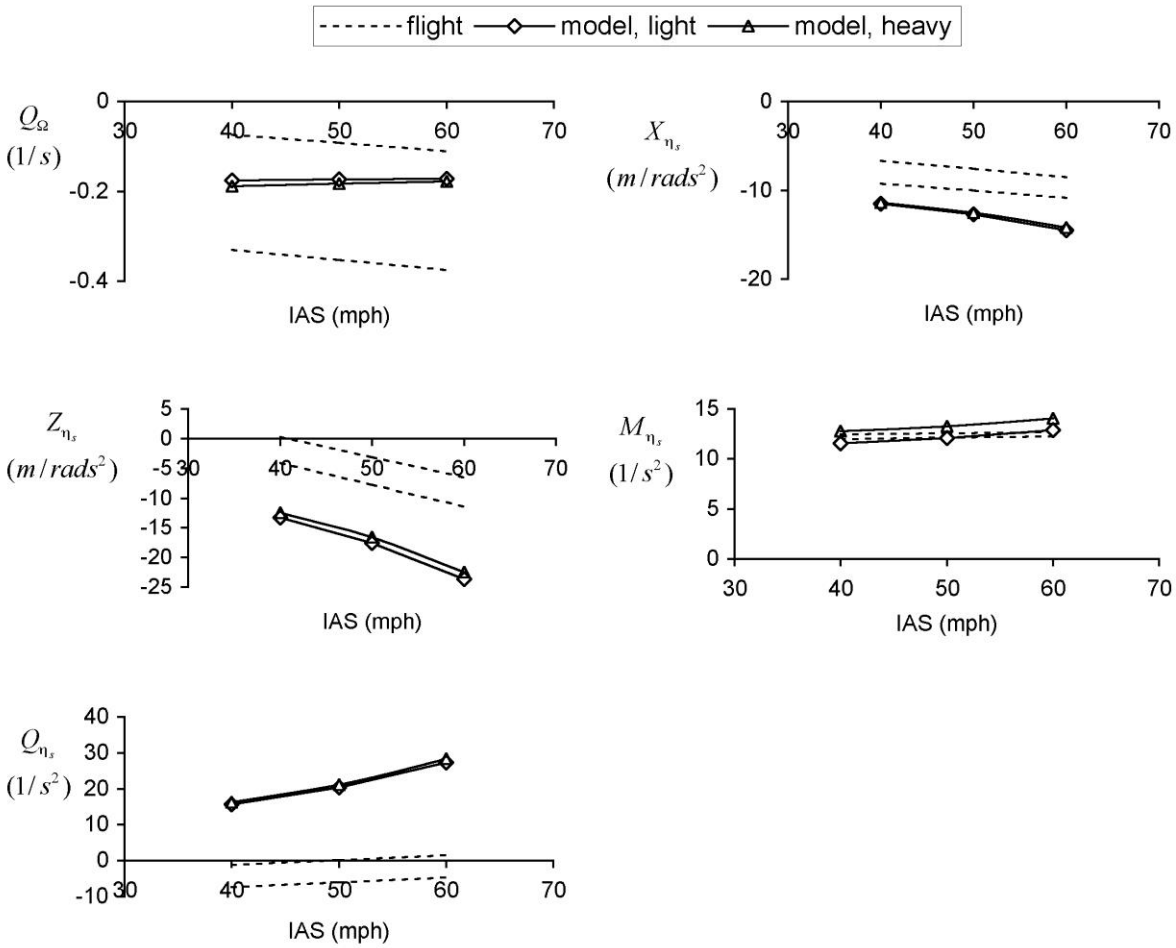

Figure 12: Comparison of Flight and Model Data, Derivatives, Montgomerie (concluded)

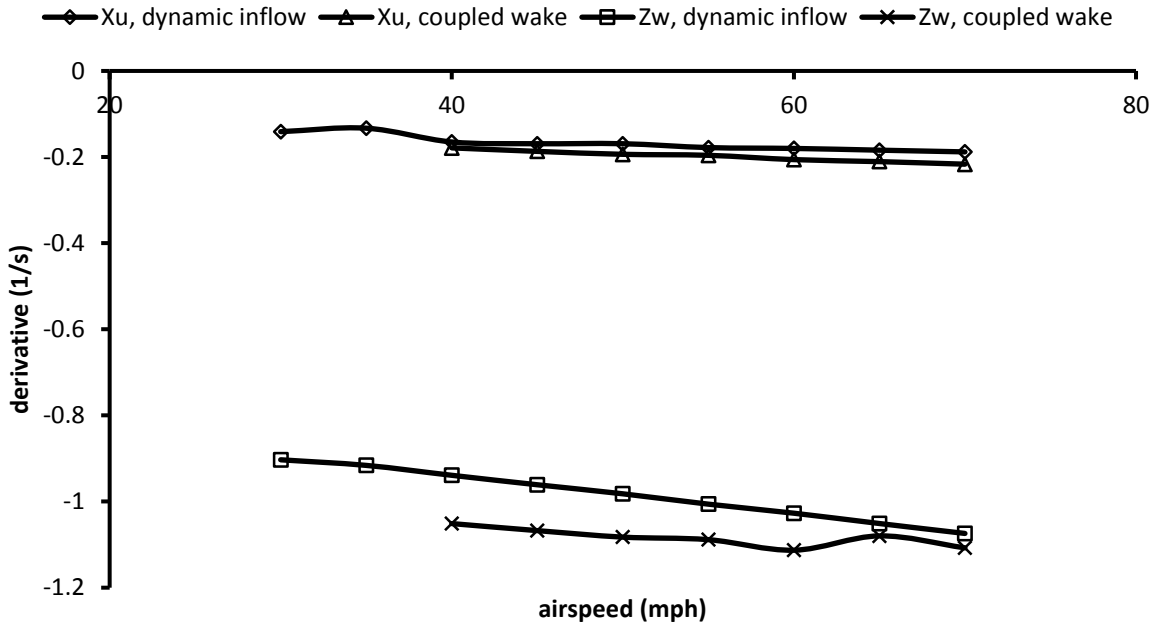

Figure 13: Drag and heave damping (X_u, Z_w) Comparisons, Dynamic Inflow & Coupled Wake, VPM M16

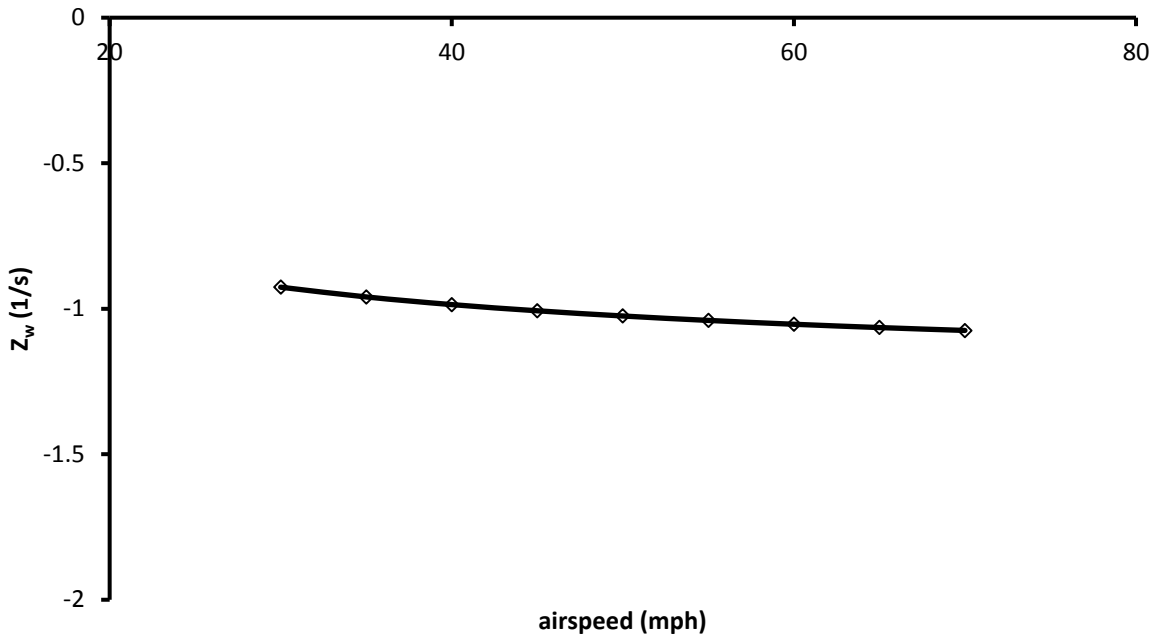

Figure 14: Heave damping (Z_w), Simple Theory, VPM M16

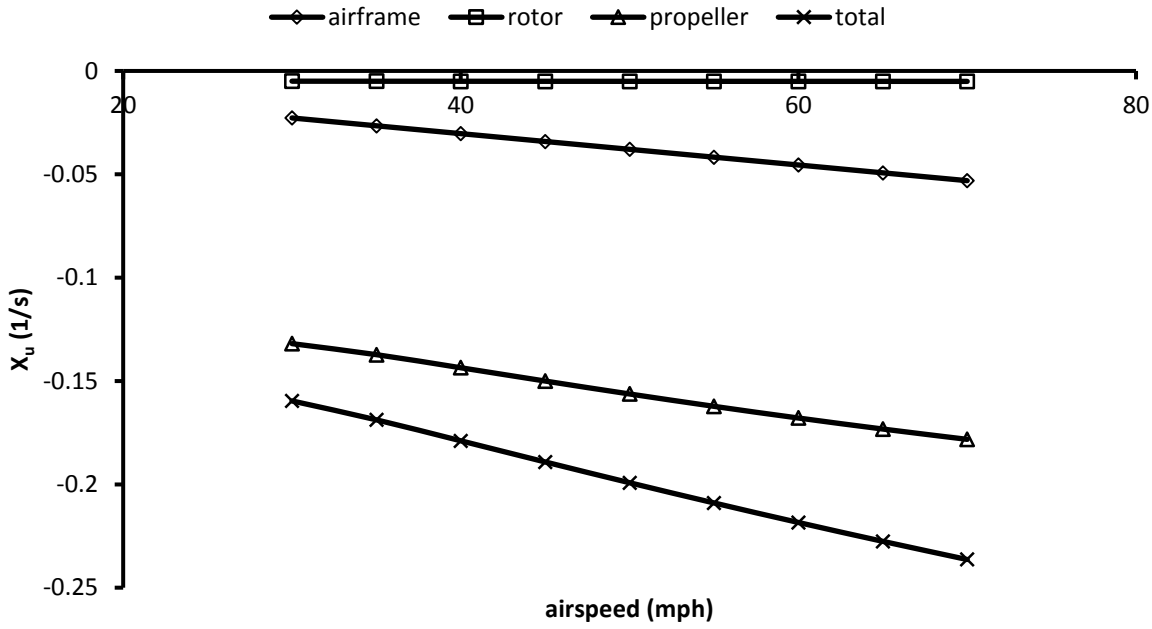

Figure 15: Drag damping (X_u), Simple Theory, VPM M16

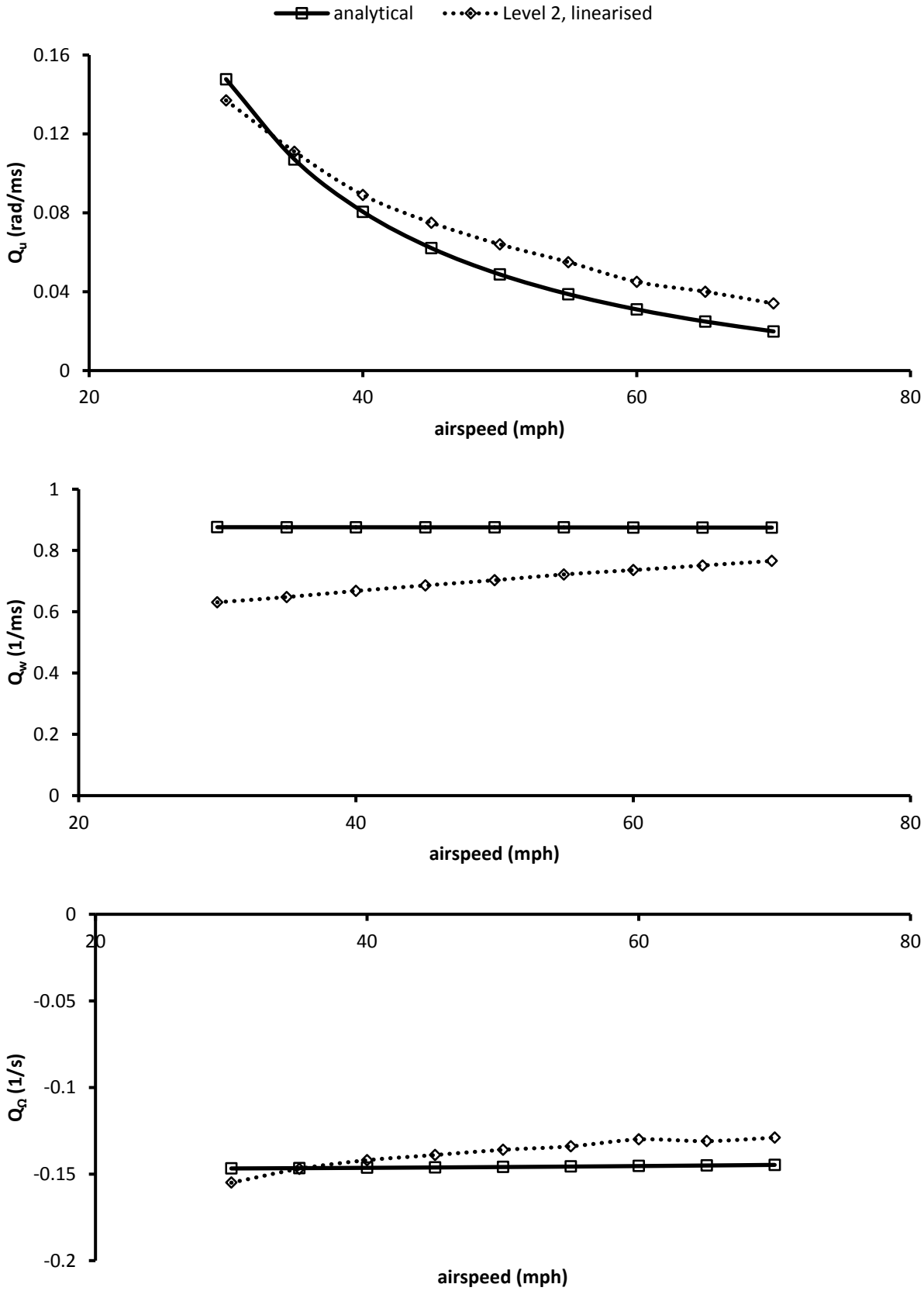

Figure 16: Rotor Torque Derivative Comparisons

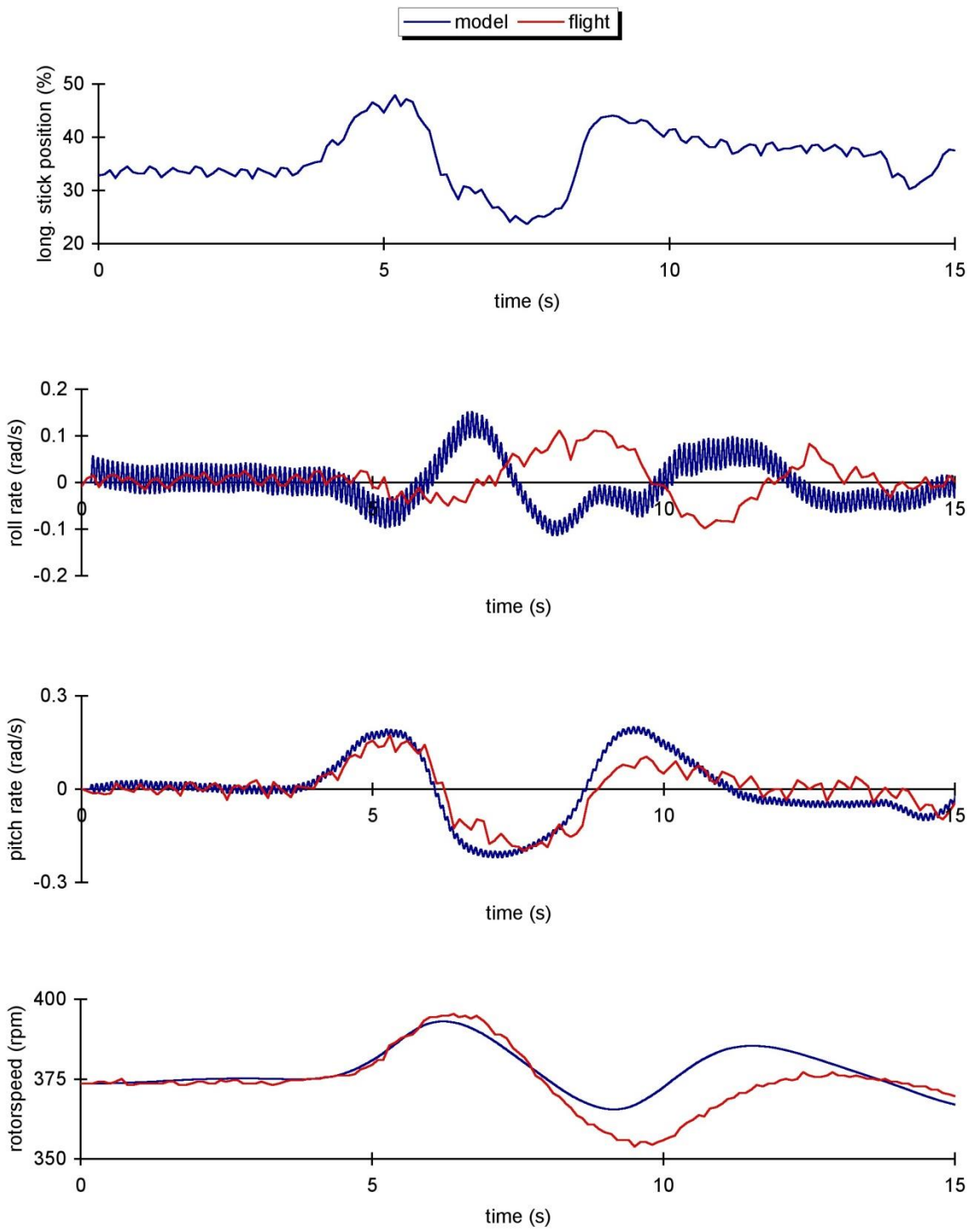

Figure 17: Non-linear Model Comparison with Flight Test

(VPM M16 Doublet Input, 70mph)

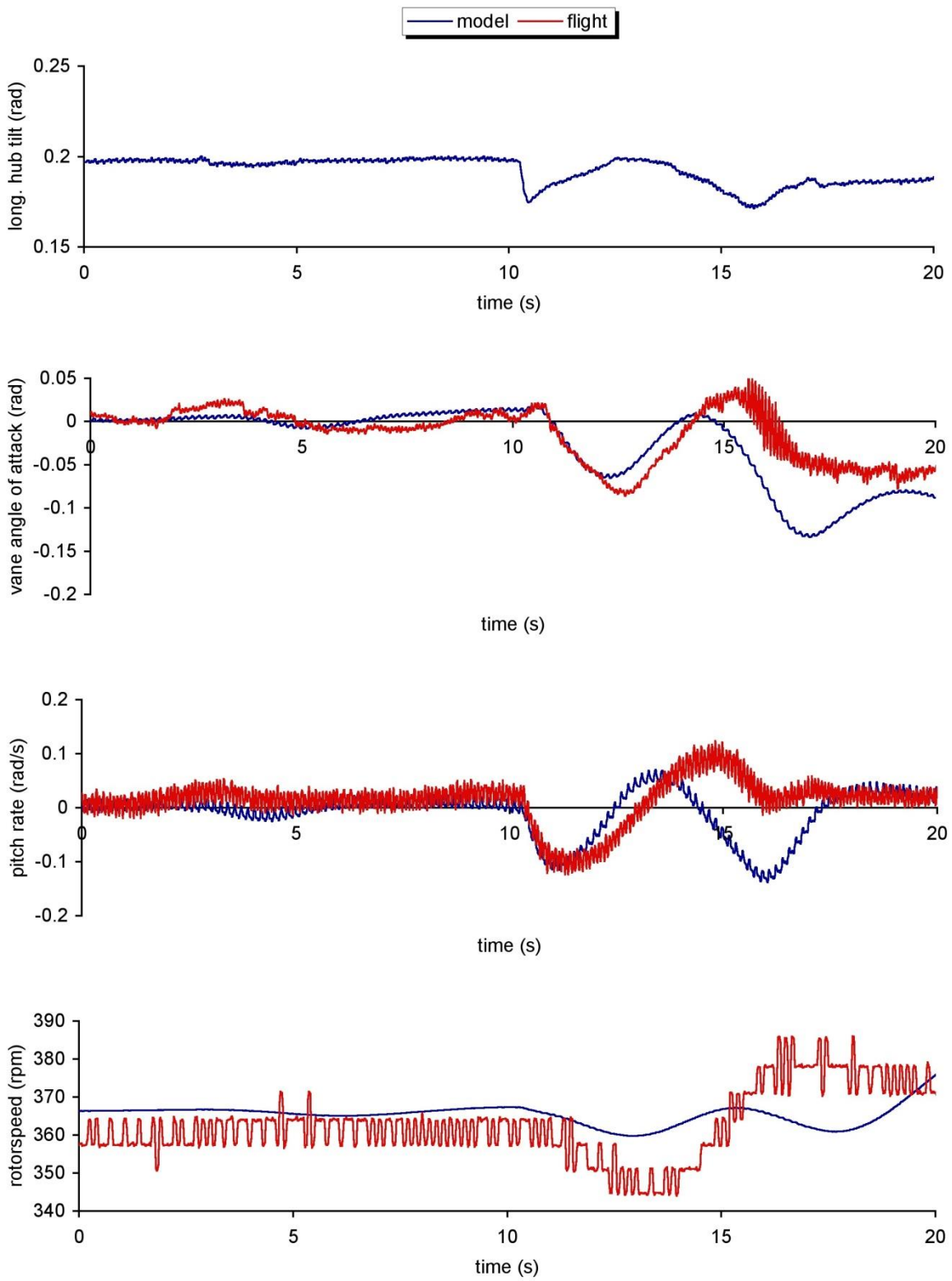

Figure 18: Non-linear Model Comparison with Flight Test

(Montgomerie Phugoid Input, 50mph)

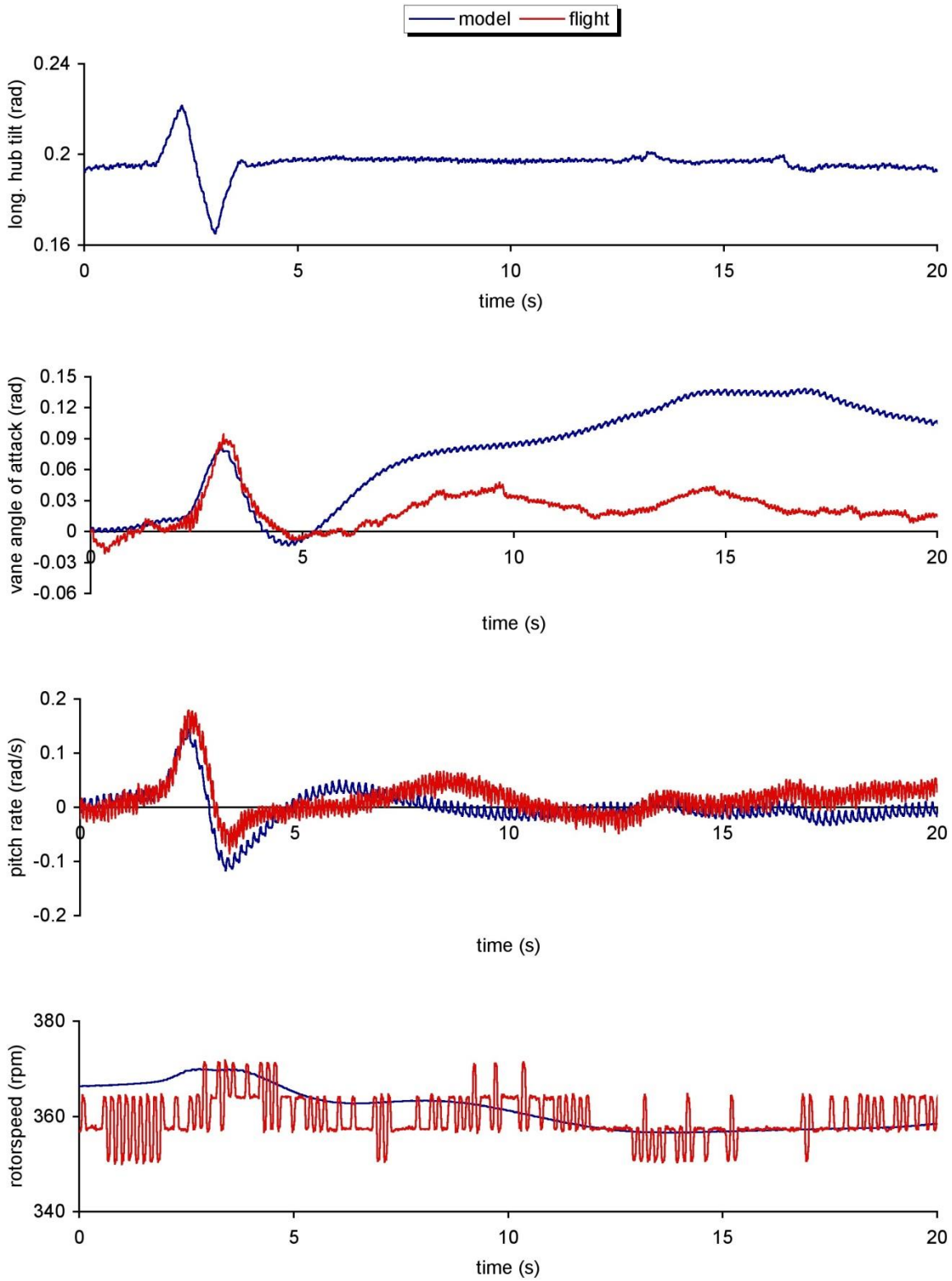

Figure 19: Non-linear Model Comparison with Flight Test

(Montgomerie Doublet Input, 50mph)

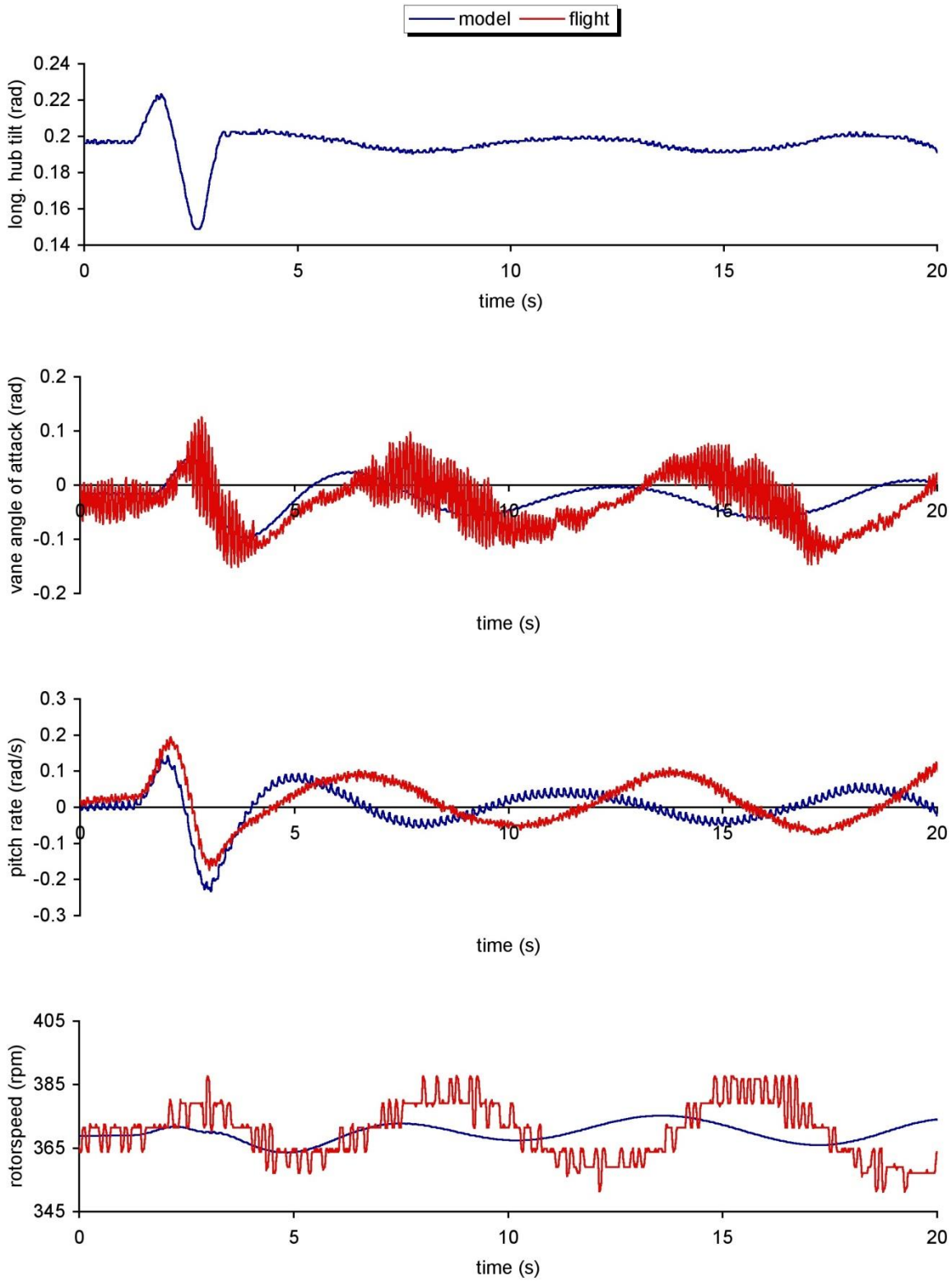

Figure 20: Non-linear Model Comparison with Flight Test

(Montgomerie Doublet Input, 55mph)